Effect of High Pressure on the Crystal Structure and Vibrational Properties of Olivine-Type $LiNiPO_4$

Enrico Bandiello,*[,1], Daniel Errandonea,[1] Julio Pellicer-Porres,[1] Alka B. Garg,[2] Placida Rodriguez-Hernandez,[3] Alfonso Muñoz,[3] Domingo Martinez-Garcia,[1] Rekha Rao,[4] and Catalin Popescu[5]

[1] *Departamento de Física Aplicada-ICMUV, MALTA Consolider Team, Universidad de Valencia, Edificio de Investigación, C/Dr. Moliner 50, Burjassot, 46100 Valencia, Spain*

[2] *High Pressure and Synchrotron Radiation Physics Division, Bhabha Atomic Research Centre, Mumbai 400085, Maharashtra, India*

[3] *Departamento de Física, Instituto de Materiales y Nanotecnología, MALTA Consolider Team, Universidad de La Laguna, La Laguna, E-38205 Tenerife, Spain*

[4] *Solid State Physics Division, Bhabha Atomic Research Centre, Mumbai 400085, India*

[5] *CELLS-ALBA Synchrotron Light Facility, Cerdanyola del Valles, 08290 Barcelona, Spain*

* Corresponding author. E-mail address: enrico.bandiello@uv.es

Abstract

In this work, we present an experimental and theoretical study of the effects of high pressure and high temperature on the structural properties of olivine-typeLiNiPO4. This compound is part of an interesting class of materials primarily studied for their potential use as electrodes in lithium-ion batteries. We found that the original olivine structure (α-phase) is stable up to ∼40 GPa. Above this pressure, the onset of a new phase is observed, as put in evidence by the X-ray diffraction (XRD) experiments. The structural refinement shows that the new phase (known as β-phase) belongs to space group Cmcm. At room temperature, the two phases coexist at least up to 50 GPa. A complete conversion to the β-phase was only obtained at high-pressure and high-temperature conditions (973 K, 6.5 GPa), as Conrey both XRD and Raman spectroscopy. Ab initio calculations support the same structural sequence. The need of high-temperature conditions to obtain the complete transformation of the α-phase into the β-phase is indicative of the existence of akinetic barrier for the phase transition. Here, we report the evolution of crystallographic parameters as a function of pressure for both phases, comparing them with the theoretical predictions. We also discuss the influence of pressure on the polyhedral units and report room-temperature equations of state. The dependence of the Raman phonons of both phases on pressure is also studied, assigning to each phonon its respective symmetry by comparison with the results of the ab initio simulations.

Introduction

Lithium compounds with the olivine structure are materials that are being actively studied from the point of view of energy storage application, in particular lithium-ion batteries. The performance of these accumulators are heavily dependent on the specific capacitance of the electrode materials. With a theoretically predicted large capacitance, orthophosphates with the LiMPO4 composition (M = Fe, Mn, Co, Ni), are promising materials to be used as cathodes in lithium-ion batteries.[1] In particular, lithium nickel phosphate, LiNiPO4, has the highest energy storage density among this family of compounds[2] and it has already been proposed for the fabrication of inexpensive, safe, and environmentally friendly Li-ion batteries with aqueous electrolytes.[3] High-pressure (HP) studies have shown to be extremely useful for characterizing the physical properties of oxides, particularly phosphates.[4–6] In the case of LiMPO4 compounds, this information has been used to understand the diffusion of Li^+ ions,[7] as it provides insights on the deformation of the structure; in turn, this has a strong influence on the possible migration pathways for the diffusion of Li^+ atoms.[8] Experiments, on the other hand, also led to the discovery of a spin transition in $LiFePO_4$.[9] Here, in order to expand the knowledge of the behavior of olivine LiMPO4 family under extreme pressure, a set of experiments have been performed on selected samples of LiNiPO4. We first characterized olivineLiNiPO4 at ambient pressure by X-ray diffraction (XRD) and Raman spectroscopy. Subsequently, similar experiments have been performed at room-temperature (RT) under compression using diamond anvil cells (DACs). Near 40 GPa, the onset of a transition to a new phase has been detected. This phase has been then synthesized under high-temperature and high-pressure conditions and characterized afterward.

It is well-known that olivine-type silicates under high pressure and temperature present a phase transition to a spinel structure.[10] Our experiments show that the olivine phase of $LiNiPO_4$ (space group *Pnma*, known as α-phase or low- pressure (LP) phase in the following) retains its original structure up to ∼40 GPa at RT. Beyond this pressure, the sudden appearance of new Bragg peaks in the XRD spectra suggests the onset of a new phase, which we have identified as Na_2CrO_4-type (space group *Cmcm*, known as β-phase or high- pressure (HP) phase in the following). These changes and the evolution of the cell parameters agree with our ab initio density-functional theory (DFT) calculations, using the generalized-gradient approximation with Hubbard parameter correction (DFT GGA+U). Previously, polymorphism has been demonstrated for the analogue olivine-type $LiCoXO_4$ compounds (X = As, P) under high-pressure and high- temperature conditions. $LiCoXO_4$ transform from the olivine structure to the spinel structure, going through an intermediate Na_2CrO_4 -like phase in a pressure range that is dependent on X.[11–13] Similarly, $LiMPO_4$ compounds with M = Fe, Co, Ni present a β-phase isostructural to that of Na_2CrO_4 under high- pressure and high-temperature conditions.[13,14] In our case, experiments performed at RT clearly show the onset of the olivine−Na_2CrO_4 transition as an effect of the applied pressure, with no hints of the spinel phase. To the best of our knowledge, this is the first report of olivine−Na_2CrO_4-type phase transition at RT as an exclusive effect of external pressure. At RT, the phase transition is incomplete: despite free-energy calculations predicting the HP phase to be the thermodynamically stable structure at a pressure slightly above 8 GPa, in the experiments, the two polymorphs coexist up to at least 50 GPa. Nonetheless, we have observed a complete transition from the olivine to the β-phase at a pressure of 6.5 GPa and a temperature of 973 K, which is indicative of the presence of a high kinetic barrier for the phase transition.

Experimental details

Polycrystalline samples of $LiNiPO_4$ were synthesized via a solid-state reaction of high-purity $Li2CO_3$, NH_4H2PO_4, and NiO (99.9%, Alfa Aesar). All three oxides were weighed in stoichiometric ratio, thoroughly mixed using a mortar and pestle, and uniaxially compressed into pellets of 13 mm diameter and 5 mm high. These compacted pellets were first heated at 375 °C for 12 h in a programmable resistive furnace with heating and cooling rates of 3 °C/min. The resultant product was crushed, ground, compacted, and heated again at 800 °C for 24 h for homogenization and better crystallization. The material was then examined by XRD (angle- dispersive mode) with a rotating anode generator as the X-ray source ($\lambda = 0.7107$ Å) and Raman spectroscopic measurements to confirm its single-phase formation.

Polycrystalline samples of $LiNiPO_4$ in the β-phase were synthesized in a Paris−Edinburgh press setup equipped with tungsten carbide anvils. Boron nitride acted as the pressure-transmitting medium for a compacted powder sample of olivine $LiNiPO_4$. An outer small graphite tube, containing the boron nitride cylinder, was used as the heating element. Two molybdenum disks, placed on the bases of the graphite oven, acted as the electrodes for the heating system. Finally, a pyrophyllite ring was used as the gasket. The sample was heated by driving a DC current across the lateral surface of the graphite tube, by means of a calibrated custom-built current−voltage setup. The synthesis of β-LiNiPO4 was performed at a pressure of 6.5 GPa and at a temperature of 973 K. The increment of the pressure was performed manually and gradually, with a relaxation time of ∼2 min after each 2 10266 Article GPa step. Once the target pressure was reached, the temperature was increased linearly from RT to 973 K for 600 s and then kept at the maximum value for 1 h. A rapid thermal quenching was performed afterward. Finally, the pressure was released and allowed to reach the ambient conditions over 48 h. The inner graphite oven was recovered undamaged by carefully cutting the pyrophyllite gasket with a small electrical rotatory cutter equipped with a diamond blade. The graphite oven and the boron nitride cylinder were then opened using a bistoury. The same tool was used to mechanically separate the polycrystalline β-$LiNiPO_4$ from the boron nitride, with the aid of an optical microscope. Small chips of the recovered sample were manually transferred to a DAC for the high-pressure studies, using a stainless needle as a spatula and, again, with the aid of an optical microscope.

High-pressure Raman measurements of the α-phase were carried out in backscattering geometry using a Mao-Bell type diamond-anvil cell (DAC). A stainless steel gasket indented to a thickness of 60 μm from an initial thickness of 200 μm with a central hole of 150 μm served as a pressure chamber. A methanol−ethanol mixture with a 4:1 ratio was used as the pressure-transmitting medium (PTM). For pressure calibration,15 fine balls of ruby (1−2 μm in diameter) were loaded in the gasket hole, along with the sample and the PTM. Optical phonons of the sample were excited using a 532 nm laser line with a power of 5 mW. Scattered light was analyzed using a 0.9 m single monochromator, coupled with an edge filter and detected by a cooled charge-coupled device (CCD). The entrance slit was kept at 50 μm. The resolution of the system was 2 cm^{-1}.

The Raman spectrum of β-LiNiPO4 was measured with a custom setup, using a 638.2 nm helium−neon laser as the excitation source. A backscattering geometry was used and a Jobin−Yvon spectrometer, in combination with a thermoelectric-cooled multichannel CCD detector and an edge filter. The spectral resolution of the setup is below 2 cm^{-1}. We performed the HP experiments

using a membrane DAC equipped with 500 μm culet diamonds. Ne was used a pressure medium and pressure was determined using ruby fluorescence.[15]

High-pressure angle-dispersive powder X-ray diffraction (XRD) experiments were performed at RT employing an Almax−Boehler DAC (diamond culets of 280 μm). The sample was loaded in a 90 μm hole drilled on a tungsten gasket preindented to a thickness of 30 μm. The ruby fluorescence method[14] was used for pressure determination. A 16:3:1 methanol−ethanol−H_2O mixture was used as PTM. Experiments were performed at the BL04-MSPD of ALBA Synchrotron.[16] We used a monochromatic X-ray beam (λ = 0.4246 Å) focused to a 10 μm × 15 μm spot. XRD patterns were collected with a Rayonix CCD detector. Structural analyses were performed with PowderCell.[17]

Calculation details

First-principles simulations were performed in the framework of the density functional theory (DFT),[18] using the Vienna ab initio simulation package (VASP).[19,20] The calculations were performed with the projector augmented wave scheme (PAW)[21] and the pseudopotentials method. In order to include the exchange-correlation energy, we have used the generalized gradient approximation (GGA) with the Perdew− Burke−Emzerhof (PBE)[22] prescription. To take into account the strong correlation of valence 3d Ni electrons, the Dudarev's[23] GGA+U method was employed with an effective U value of 5.1 eV, as suggested in ref 24. To achieve highly converged results, we have extended the plane basis setup to an energy cutoff of 520 eV. The integrations over the Brillouin zone (BZ) were made with a dense Monkhorts−Pack special k- points grid to ensure good convergence. At selected volumes, the structural configurations were fully optimized through the calculations of the stress tensor and the forces on the atoms. Our optimization criterion was to relax the configuration until the stress tensor deviations from the diagonal form were <0.1 GPa, and the forces on the atoms were <0.006 eV/Å. Through this process, with the DFT methodology employed, the stress for each volume and so the theoretical pressure $P(V)$ are also obtained. The set of accurate results of energy (E), volume (V), and pressure (P) data, provided by calculations allowed us to derive the $P-V$ equation of state (EOS). In our simulations, we found that the antiferromagnetic configuration has the lowest energy. Temperature and zero-point motion effects were not included in these simulations. Lattice vibrations calculations were performed in order to obtain the phonons at the zone center (Γ point), using the direct force-constant approach.[25] In order to obtain the dynamical matrix at the zone center, we need highly accurate calculations of the forces on the atoms when fixed small displacements from the equilibrium configuration of the atoms are considered. The crystal symmetry helps to reduce the number of independent displacements needed to obtain the dynamical matrix. Diagonalization of the dynamical matrix provided the symmetry, polarization vectors, and phonon frequencies, as well as the irreducible representation and the character of the phonons at Γ.

Results and Discussions

Characterization at ambient pressure. On a first visual inspection, fine powders of α-$LiNiPO_4$ showed a pale yellow-green color. The structure of lithium nickel phosphate under ambient con-

ditions belongs to space group Pnma. It is a tridimensional (3D) network of distorted NiO_6 octahedral units, sharing corners with NiO_6 octahedra and being cross- linked by irregular PO_4 tetrahedral units. Lithium atoms, in 6-fold coordination with oxygen, occupy the voids in a 3D network, along the (010) and (001) directions.[26] A schematic representation of the orthorhombic olivine-type $LiNiPO_4$ is shown in Figure 1 (left). Summarized in Table 1 are the calculated atomic positions in the unit cell for the olivine $LiNiPO_4$, which agree within <1.2% with previous experimental results obtained from single-crystal XRD data.[27] The powder XRD spectrum for the LP phase of $LiNiPO_4$ under ambient conditions is shown in Figure 2a. Rietveld refinement of the aforementioned spectrum gives unit-cell parameters agreeing within 0.2% with previously reported values,28 with quality factors as low as R_p = 0.48%, R_{wp} = 1.41%, and R_{exp} = 1.43%. At the same time, calculated unit-cell parameters agree within 1% with our experimental results (see Table 2). This is indicative of the suitability of DFT for the accurate description of $LiNiPO_4$ structure, suggesting that it is a powerful tool to predict other physical properties and to complement the experimental characterization of lithium nickel phosphate under pressure.

The Raman spectrum of olivine-type $LiNiPO_4$ under ambient conditions is shown in Figure 3, with a comparison of the positions of the predicted and observed Raman modes. The group representation corresponding to the lattice modes at the center of the Brillouin zone can be decomposed as $\Gamma = 11A_g + 7B_{1g} + 11B_{2g} + 7B_{3g} + 10A_u + 14B_{1u} + 10B_{2u} + 14B_{3u}$.[28,29] Even modes are Raman active. The acoustic modes have B_{1u}, B_{2u}, and B_{3u} symmetry. Thirty-five (35) modes –13 B_{1u}, 9 B_{2u}, and 13 B_{3u} – are IR active. Finally, A_u modes are silent. In our experiments, only 24 Raman modes out of the 36 Raman active modes are detected, in agreement with previous studies.[14] The frequency of the measured modes, as well as the results of the ab initio computations, are compiled in Table 3. Calculated Raman modes are nonuniformly shifted with respect to the experimentally detected phonons. However, the differences between measured and calculated frequencies are within a 5% range, which is typical of DFT calculations.[30] The symmetry assignment of the Raman-measured modes is based on the work performed with single crystals in ref 31 and also by direct comparison with the calculations. The correctness of this approach has been confirmed later when the pressure evolution of the experimentally detected Raman modes has been compared with the one predicted by the calculations (see Figure S5 in the Supporting Information). We also provide the frequencies and assignation of the infrared (IR) active modes in Table S1 of the Supporting Information. The Raman spectrum of LiNiPO4 can be clearly separated into two different regions: one below 400 cm^{-1} and one above 1400 cm^{-1} . These regions correspond, respectively, to the domain of the internal and external modes of the $(PO_4)^{3-}$ anion. Internal modes are related to the displacement of oxygen atoms in the tetrahedral units, while external modes consist of librations of the PO_4 units and of translations of Li, Ni, and PO_4. This mode separation is an approximation that has already been successfully used to describe the vibrational spectra of other olivine orthophosphate compounds.[31] The modes of the PO_4 tetrahedron are labeled ν_1 (symmetrical stretching, A_1), ν_2 (bending, E), ν_3 (T_2), and ν_4 (T^2). According to Frost et al., their wavenumbers in an isolated anion are ν_1=938 cm^{-1}, ν_2=420 cm^{-1}, ν_3=1017 cm^{-1}, and ν_4=567 cm^{-1}.[32] The correlation between the $LiNiPO_4$ modes and the tetrahedron modes, according to group theory, has been established in ref 31. Our calculations confirm that the main features of the phonon patterns of even modes with wavenumbers of >400 cm^{-1} can associated with the internal modes. The specific relationships are described in Table 3.

The six modes with larger wavenumber correspond to ν_3 modes. One of them is reported to be situated at 953 cm^{-1}.[31] It is not possible to observe it in a powder spectrum, because of its closeness to the most intense peak located at 948 cm^{-1}, which is the totally symmetric A_g (ν_1). In addition, according to calculations, the other symmetric mode, B_{2g} (ν_1), is degenerate with A_g (ν_1). This is why it is not observed neither in single crystals nor in the present experiment. As we willdiscuss in the next section, this high-frequency mode broadens when HP is applied. This is consistent with considering it as a doublet since the B_{2g} (ν_1) and A_g (ν_1) modes would probably have slightly different pressure coefficients. In fact, our calculations predict a slight larger hardening for the B_{2g} (ν_1) mode than for the A_g (ν_1) mode, as can be seen in Table 3.

The structures observed between 680 and 800 cm^{-1} do not correspond to phonon modes. Their intensity increases in sample zones with more intense orange color. We suggest that the Raman structures in this range are related to defects. The tetrahedral ν_4 modes are observed between 582 cm^{-1} and 640 cm^{-1} . We observe the B_{2g} (ν_4) mode at 650 cm^{-1} , which has not been characterized in previous experiments. Finally, modes observed from 418 cm^{-1} to 467 cm^{-1} correspond to ν_2 modes. Remarkably, Li atoms are not allowed to move during Raman-active vibrations, because Li atoms occupy 4a sites, which are inversion centers for the olivine structure (see Table 1). Raman-active modes are only those of the even species, so no Raman activity is expected from Li atoms. This has been verified experimentally by García-Moreno et al. by showing that the Raman spectrum of olivine LiNiPO4 is unaffected upon substitution of the lithium isotope ^7Li with ^6Li.[14] Similar results were obtained by Ramana et al., who observed only minor changes in the Raman spectra of LiNiPO4 upon delithiation.[29] The distinction between internal and external modes is not so clear in odd modes, where Li atoms contribute to the phonon patterns. The frequency of the external modes increases.[31] As an example, the highest-energy mode is the $B_{1u}(\nu_3)$ mode at 1088 cm^{-1} , where Li has a small amplitude. In the rest of ν_3 and ν_1 odd modes, there is no significant Li movement, whereas in ν_4 modes, the Li contribution is remarkable. The separation between internal and external modes is not clear in ν_2 odd modes.

High-pressure Studies. High-pressure experiments on our samples started with powder XRD experiments at RT up to ~50 GPa (see Figure 2a). In the range up to 39.7 GPa, the only remarkable changes in the XRD spectra are represented by the monotonic shift of the Bragg reflections toward higher values of 2θ, because of the reduction of the cell parameters. The original phase of $LiNiPO_4$ is thus retained across this pressure range. Rietveld refinements have been performed, keeping the atomic positions given in the literature as constant parameters (see Table 1), independent of the pressure. The aforementioned XRD patterns could be successfully fitted to the orthorhombic α-phase of LiNiPO4 (LP phase). The quality factors for the refinement are similar from ambient pressure up to 39.7 GPa. The experiments support the absence of either phase transitions or chemical decomposition in this pressure range.

From the structural refinements, we determined the variation of the unit-cell parameters under compression. The results are shown in Figure 4. Experimentally, all the parameters decrease with pressure; at 39.7 GPa, parameters *a*, *b*, and *c* are contracted to 8.89(1) Å, 5.39(1) Å, and 4.32(1) Å, respectively, which implies a normalized variation of 12.2%, 8.2%, and 8.0%. Therefore, the compressibility of α-LiNiPO4 is anisotropic, being the lattice more compressible along the [100] direction than the [010] and [001] directions. The relative volume variation at 39.7 GPa is 28.2%. Noteworthy, DFT calculations predict an almost-identical trend, despite a slight overestimation of the experimental values; the latter could be related to nonhydrostatic effects which develop above

10 GPa.[33] Results from calculations are compared with experiments in Figure 4. Similar to what happens for the olivine phase of the analogue $LiFePO_4$ compound, the anisotropic compressibility of lithium nickel phosphate can be attributed to the nonuniform evolution of the interatomic distances, as calculated by means of DFT.[34] Given the consistency between experiments and calculations, the DFT simulations can be used to obtain accurate information on bond distances and their pressure dependence.[35] As clearly visible in Figure 5a, the effect of the pressure on the length of P−O bonds is rather limited, while Li−O and Ni−O bonds are shortened by a much greater extent and the distortion of different polyhedral units being enhanced by compression. The volume of the corresponding polyhedra varies accordingly, as demonstrated by the calculated pressure−volume relation of the LiO_6 and NiO_6 octahedra and the PO_4 tetrahedron (Figure 5b). The predicted relative volume variations at 40 GPa are 29% (LiO_6), 21% (NiO_6), and 7% (PO_4). The incompressibility of the PO4 tetrahedron is consistent with the results obtained in other phosphates.[36] The contraction of the unit-cell volume under compression is mainly caused by the volume reduction of the LiO_6 and NiO_6 octahedral units.

The experimental volume−pressure results can be represented by a third-order Birch−Murnaghan equation of state (EOS).37 The fitting leads to a calculated bulk modulus B_0= 94(2) GPa, with the first derivative being B_0' = 2.9(5). These values are compatible with those predicted and measured for analogue $LiMPO_4$ olivine materials.[24,34] For instance, the bulk modulus of $LiFePO_4$ is 91.7 GPa.[34] Our and previous results suggest that olivine-type phosphates have a bulk modulus smaller than olivine-type silicates, in which B_0 > 119 GPa.[38−42] The initial unit-cell volume, calculated from the Birch− Murnaghan EOS, is V_0 = 275.5(5) Å3, in good agreement with the experimental value of 274.9(1) Å3. The implied value43 of the second pressure derivative of the bulk modulus is −0.0425 GPa^{-1} .

When increasing pressure at RT above 39.7 GPa, at 40.9 GPa, the XRD patterns change as new Bragg reflections appear, being those at 2θ ≈ 6°, 6.5°, 7.4°, and 10.6°, the most prominent (denoted by asterisks in Figure 2a). These new peaks monotonically increase in intensity with pressure (see Figure S1 in the Supporting Information) and are independent of those of the original structure. This is a clear indication of the onset of a phase transition and the coexistence of the two polymorphs. The incipient phase has been assigned to the β- phase, Cmcm space group. This assumption is corroborated by the Rietveld refinement reported in Figure 2a, performed for a mixture of the α and β phases at 49.8 GPa. The XRD pattern of LP phase is still dominant and unaffected by the extreme pressure, except for the expected shift of the peaks toward higher values of 2θ. Upon release of the pressure, a very small hysteresis can be appreciated in the diffractogram, in particular a general broadening of the peaks and extremely weak reflections not present in the original data but which can be related to those observed at 49.8 GPa (see Figure S2 in the Supporting Information). As shown in Figure 1 (right), the structure of β-LiNiPO4 consists of rows of edge-sharing NiO6 octahedra running along the [001] axis that are cross-linked by LiO_4 and PO_4 tetrahedral units along the [100] axis. There is a striking similarity of the $LiNiPO_4$ structure with that of $AlPO_4$.[44] In $LiNiPO_4$, however, there are four chemical elements instead of three. Ni plays the role of Al, whereas Li and P tetrahedral alternate along the c-axis. The arrangement can be understood as originated by oxygen valence require- ments. The substitution of Al^{3+} by Ni^{2+} requires the contribution from Li^{1+}. In the β-$LiNiPO_4$ structure, O atoms are connected to one Ni^{2+} atom, one Li^{+} atom, and one P^{5+} atom.

Raman spectra for α-$LiNiPO_4$ at RT have been measured under pressure up to 12.2 GPa (Figure S3 in the Supporting Information). The spectra show a gradual evolution with pressure with no evidence of structural changes, in agreement with XRD experiments. There are three modes that were not detected when the sample was under compression in the DAC. These are the modes denoted by an asterisk in Table 3. In addition, there are three modes that become very weak and difficult to follow at a pressure beyond 5 GPa. These are the internal modes originally situated at 417.5, 437.0, and 599.6 cm^{-1} . The remaining 17 Raman-active modes can be followed up to 12.2 GPa. We found a generalized hardening of all Raman modes (see Figure 6). We also found that the pressure dependence of the phonon frequency is not linear, as it can be described with a quadratic function. The results of the fits are shown in Table 3. The calculated pressure dependence of all Raman-active modes is represented in the Figure S4 in the Supporting Information. Under compression, there are several modes that gradually merge and a phonon crossing for phonons of different symmetries with frequencies just above 400 cm^{-1} . A good agreement is found between experiments and calculations for the pressure dependence of the modes.

DFT calculations[34] predicted a phase transition at RT from the α-phase to the β-phase for the analogue compound $LiFePO_4$ at pressures below 10 GPa. However, experiments did not find it up to pressures of 22 GPa.[34] In our experiment, a complete and irreversible conversion of $LiNiPO_4$ to the β-phase has been only obtained under the combined application of high-pressure and high-temperature conditions (6.5 GPa and 973 K). To complement our study, we have calculated the enthalpy of the α- and β-phases at different pressures to determine the theoretical transition pressure. The results are shown in Figure 7. According to the present ab initio DFT calculations, the β-phase of $LiNiPO_4$ is expected to be thermodynamically more stable than the LP phase above 8 GPa. Calculations not only show that the β-phase has a lower enthalpy than the α-phase, but also that the HP phase is dynamically and mechanically stable (there are not imaginary phonon modes[45,46] and the elastic constants verify the generalized Born stability criteria). [47] The incomplete conversion to the HP phase at room temperature, even at pressures six times higher than that predicted by DFT, can be thus safely attributed to a high kinetic barrier associated with the phase transition. Such phenomenon has been previously observed in other phosphates (e.g., $AlPO_4$)[44] and it is fully consistent with the fact that we obtained a complete and stable transition of the material to the β-phase under high- temperature and high-pressure conditions, specifically 973 K and 6.5 GPa. As a sidenote, we needed to lower the maximum temperature used during the synthesis, with respect to information in ref 14, since decomposition of the starting material was observed when synthesis was attempted at the previously reported temperature of 1173 K.[14] Nonetheless, at the extent shown by our XRD and Raman experiments (in the following), the phase synthesized by us and the phase synthesized previously by other authors14 under different

conditions are identical. The hindering of the transition by the kinetic barrier is consistent with the first-order nature of the α−β transition,[36] which has associated a volume collapse of 3%. It is important to remark that the coexistence of both phases at room temperature under high-pressure conditions is not due to the nonhydrostaticity of the pressure medium, but rather to the very nature of the transition and its high kinetic barrier. The same phenomenon is in fact observed independently of the pressure medium, being methanol:ethanol or argon, in the analogue $HoVO_4$ oxide for a first-order zircon−scheelite with a high energetic barrier.[48] Regarding a possible second phase transition to a spinel-type structure as found in olivine-type silicates,[49] no evidence of it has been found in our Raman and XRD experiments. In addition, our calculations found that spinel-type

$LiNiPO_4$ has a larger enthalpy than the α- and β-polymorphs in the pressure range of interest of our study. Therefore, the transition to spinel-type $LiNiPO_4$ is not expected to occur up to 50 GPa. This is probably because the strong covalent character of the P−O bond is expected to delay (in comparison to silicates) the high- pressure phase transition to a phase in which phosphor is 6- fold coordinated. Indeed, a single phase with six-coordinated phosphor has been observed in $AlPO_4$ only beyond 75 GPa.[44]

The identification of the phase obtained at HP, HT comes from XRD (Figure 2b) and Raman spectroscopy (see Figure 8 and Table 4), which successfully replicate already reported ambient-pressure results for β-$LiNiPO_4$.[14] The agreement for the crystal structure is good between calculations and experiments (see Tables 5 and 6). The mechanical decomposition of the lattice vibrations is given by $\Gamma = 6\,A_g + 5B_{1g} + 2B_{2g} + 5B_{3g} + 3A_u + 7B_{1u} + 8B_{2u} + 6B_{3u}$. Of these modes, the Au modes are silent and three modes are acoustic ($B_{1u} + B_{2u} + B3_u$). Calculations allowed us to assign the phonon symmetry of different Raman modes. They also provide the pressure dependence of Raman modes, which, for the sake of completeness and to facilitate the comparison in future studies, is included in Figure S7 in the Supporting Information. Our ab initio simulations also give information on the IR-active modes, which are included for completeness in Table S2 in the Supporting Information. Note that, of the 18 Raman-active modes ($6A_g + 5B_{1g} + 2B_{2g} + 5B_{3g}$), 14 have been measured (i.e., one mode more than in previous studies).[14] Regarding the IR-active and acoustic modes, there are no results available in the literature to compare with the frequencies of the 18 modes calculated ($6B_{1u} + 7B_{2u} + 5B_{3u}$). We hope that our calculations will trigger such experiments.

Since the β-$LiNiPO_4$ phase is still based on PO4 tetrahedral units, it would seem logical to apply the same classification of internal and external modes as in α-$LiNiPO_4$. Despite that, the ab initio calculations yield phonon patterns that do not agree with this classification. As an example, there is no mode with pure ν1 stretching behavior. The mode with the appropriated symmetry at the expected frequency is the Ag mode at 877.9 cm^{-1}. However, its phonon pattern shows a P atom amplitude, comparable to those of O atoms, and a mixed bending− stretching behavior. The mode attribution performed in ref 14 then is not valid. The different behavior of the β-$LiNiPO_4$ polymorph is understood to be associated with a high-pressure phase where the electronic charge is expected to be more delocalized. Specifically, the alternation of P and Li tetrahedra increases the interconnection of PO_4 units with the entire lattice. In addition, it is interesting to describe another difference between lattice vibrations in the α- and β-phases of β-$LiNiPO_4$. In α-$LiNiPO_4$, the inversion center located at Li sites forces them to be present in even modes, whereas in β- $LiNiPO_4$, the Ni atoms are the ones that do not participate in even modes, given the 2/m symmetry of their Wyckoff position.

We have also obtained information on the pressure dependence of most of the Raman modes of the synthesized β-$LiNiPO_4$. In Figure S6 in the Supporting Information, we show Raman spectra measured at different pressures. From these same spectra, we obtained the pressure dependence of some of the modes. The results are shown in Figure 9. The calculated pressure dependence of the different modes is given in Figure S7 in the Supporting Information. In Table 4, the pressure coefficients of different modes are compared. The agreement between theory and experiment is similar for the β- phase than for the α-phase (also see Figure S8 in the Supporting Information for a graphical comparison). From the 14 modes, we observed, for the β-phase, that only 9 were detectable when loaded into the DAC. In addition, the mode at 619 cm^{-1} becomes undetectable for

pressures of $P > 10$ GPa. All the detected modes harden upon compression, with no other significant changes (no crossing, no splitting). As also shown by XRD, no further phase transitions are detected in this pressure range. This agrees with enthalpy calculations suggesting that a subsequent transition to a spinel phase is not energetically allowed. Calculations also show that the β-phase is dynamically stable. In most modes, the linear pressure coefficient of Raman modes (see Table 4) is ∼2−5 cm^{-1} GPa^{-1}. The exception is the mode at 565 cm^{-1} (with a linear coefficient of 0.66 cm^{-1} GPa^{-1}). According to García-Moreno ´et al.,[14] this mode is assigned to an internal vibration of the phosphate anion. Its low pressure coefficient suggests the existence of very stiff P−O bonds in this phase, which is in agreement with conclusion obtained from XRD. Unlike in the olivine-type phase, vibrations of the Li atom are Raman active in β-$LiNiPO_4$. The mode associated with this vibration correspond to modes at 185, 343, 497, and 646.7 cm^{-1}.

Nonetheless, only the mode at 646.7 cm^{-1} can be followed when the sample is in the DAC. This mode is the only one that has nearly linear pressure dependence. From calculations, we have obtained the pressure dependence of IR-active and acoustic modes. For completeness, these results are reported in Table S2 in the Supporting Information. Interestingly, there is an IR-active mode and one Raman-active mode which gradually soften under compression; however, their frequency does not become imaginary in the pressure range of stability of the β-phase. It means they are not proper soft modes.[50] A detailed study of them is beyond the scope of this work.

Further insights of the behavior of the synthesized β-phase phase under compression come from XRD analysis. We have collected XRD patterns at different pressures up to 14.9 GPa (Figure 2b). We found that the β-phase remains stable in this pressure range. Also, in this case, as we did in the case of the α- phase, the atomic positions were not refined. Their values, given in Table 5, have been kept fixed at the values given by Garcia-Moreno et al.14 The unit-cell parameters under ambient conditions for this phase are a = 5.358(1) Å, b = 8.127(1) Å, and c = 6.124(1) Å, in full compatibility with previously reported values for β-LiNiPO*4* (see Table 6).14 These values also agree with our calculations. At 14.9 GPa, the unit-cell parameters decrease to 5.112(1), 7.849(1), and 5.841(1) Å, respectively, with relative variations of 2.4%, 1.7%, and 2.4%, respectively. The compressibility is slightly anisotropic, but to a much lower extent than that of the α-phase. The dependence of the unit-cell parameters on pressure is shown in Figure 10.

The values for the synthesized β-$LiNiPO_4$ (0−14.9 GPa) and for the same polymorph in the range of coexistence of the α- and β-phases (40−50 GPa) are included in the figure. Results in the range of 40−50 GPa are less accurate, as unit-cell parameters were determined from XRD patterns, evidencing phase coexistence. Consequently, in order to determine the compressibility, we used only the results from 0 to 14.9 GPa. The bulk modulus determined by limiting the fitting of the third-order Birch−Murnaghan EOS51 to the lowest pressure range is B_0 = 88(2) GPa with B_0' 0 = 3.5(5). The initial volume obtained from the fit is V_0 = 267.3(6) $Å^3$, which is compatible with the value of 266.7(2) $Å^3$ given by the direct measurement. The bulk modulus is slightly smaller than that of the α-phase, but its pressure derivative is slightly larger. Since both parameters are correlated,[51,52] it is not possible to discern which polymorph is more compressible. If a second-order EOS is used (B_0' = 4), for both structures, we obtain B_0 = 86(3) GPa, which indicates that, within uncertainties, they have the same compressibility. This is consistent with the fact that an identical volume change (12%) occurs in both structures from 0 to 15 GPa. The obtained bulk moduli are comparable with those previously reported for $LiFePO_4$.[25,53] This suggests that similar bulk moduli can also be expected for related compounds, such as $LiMgPO_4$.[54] Interestingly, the extrapolation of the fit curve

beyond 14.9 GPa seamlessly connects the experimental pressure−volume data in the 40−50 GPa region, despite the large pressure gap in the experimental data. As mentioned previously, the $P-V$ values of Figure 10 in the highest pressure range are calculated from the cell parameters of the supposed β-phase by simultaneously refining the two phases observed when pristine $LiNiPO_4$ (i.e., the original α- phase) is compressed at $P > 40$ GPa at RT (see also Figure 2a and Figure S1). Despite the large gap in the experimental data, the same EOS is able to describe the synthesized β-phase at low pressure and the high-pressure phase is observed to coexist with the α-phase. We believe that this is further confirmation that these two phases are actually the same structure.[55] The same behavior is evident for the individual parameters in Figure 10. Finally, ab initio DFT correctly predicts the observed trends, even if the experimental values are increasingly overestimated at higher pressure.

Conclusions

In this work, we have reported an experimental and theoretical study of olivine-type $LiNiPO_4$ (Pnma, α-$LiNiPO_4$) under compression. At room temperature, the onset of a transition to a new phase (Cmcm, β-$LiNiPO_4$) has been detected by X-ray diffraction experiments at a pressure of ∼40 GPa. The two phases, α and β, coexist up to at least 50 GPa. A complete α-to- β phase transition has not been achieved at room temperature. Nonetheless, to the best of our knowledge, this is the first time that an incipient phase transition for $LiMPO_4$ (M = Fe, Mn, Co, Ni) is reported as the effect of the applied pressure only. Theoretical calculations predict the same phase transition starting at ∼8 GPa. The pressure delay observed exper- imentally is attributed to the existence of an energy barrier for the transition. Indeed, a complete and irreversible α-to-β transition could only be obtained under high-pressure and high-temperature conditions, by annealing the sample at 973 K at a pressure of 6.5 GPa. This confirmed the existence of the kinetic barrier. Moreover, the β-phase observed at high pressure and room temperature (RT) and of the β-phase obtained at high pressure and high temperature obey the same EOS, thus confirming that they are the same structure. The evolution of the crystallographic parameters for both the α- and β-phases has been reported, along with the evolution of their Raman modes. The mode assignment and pressure dependence of different modes were also discussed. Ab initio DFT calculations also gave information on IR modes. From the pressure dependence of the unit-cell volume, we determined the bulk modulus and its derivative for both structures. The compression of both phases is anisotropic. The value of B0 for the LP phase has been determined to be compatible with previously reported experimental and theoretical values for analogue $LiMPO_4$ compounds. Both phases are found to have similar compressibility. Finally, the relationship between bulk and polyhedral compressibilities have been explored, revealing that the Li−O and Ni−O bonds are much more compressible than P−O bonds, controlling the volume change of the crystal structure.

Associated Content

The Supporting Information is available free of charge at xxxxxxx.

Additional IR and Raman mode calculations; high-pressure XRD patterns; Raman spectra at selected pressures (α- and β-phases); Raman modes evolution (theory and experiment comparison for the α- and β-phases)

Author Contributions

The manuscript was written through contributions of all authors. All authors have given approval to the final version of the manuscript.

Notes

The authors declare no competing financial interest.

Acknowledgements

E.B. would like to thank the Generalitat Valenciana for his postdoctoral contract (ValI+D, APOSTD2017). This research was supported by the Spanish Ministerio de Economiá y Competitividad, the Spanish Research Agency, and the European Fund for Regional Development under Grant Nos: MAT2016-75586-C4-1-P/3-P and MAT2015-71070-REDC. AM and PR-H acknowledge computing time provided by Red Española de Supercomputación (RES) and MALTA- Cluster. HP XRD experiments were performed at MSPD beamline at ALBA Synchrotron Light Facility with the collaboration of Alba staff.

Table 1. Atomic Coordinates for α-LiNiPO4 at Ambient Pressure, Space Group Pnma (No. 62); Comparison between Calculated Values and the Literature Values[26]

		Calculated			Literature		
atom	site	x/a	y/b	z/c	x/a	y/b	z/c
Li	4a	0	0	0	0	0	0
Ni	4c	0.27469	1/4	0.98791	0.27563(6)	1/4	0.9828(1)
P	4c	0.09501	1/4	0.4215	0.0944(1)	1/4	0.4177(3)
O(1)	4c	0.09864	1/4	0.74626	0.0998(3)	1/4	0.7422(8)
O(2)	4c	0.45171	1/4	0.19941	0.4517(3)	1/4	0.2011(8)
O(3)	8d	0.16708	0.04229	0.27969	0.1659(2)	0.0426(4)	0.2779(5)

Table 2. Lattice Parameters for α-$LiNiPO_4$ at Ambient Pressure, Space Group Pnma (No. 62)[a]

parameter	calculated	experimental	literature
a (Å)	10.1092	10.036(1)	10.032(1)
b (Å)	5.9077	5.856(1)	5.855(1)
c (Å)	4.7218	4.676(1)	4.681(1)
volume (Å3)	282.996	274.9(1)	274.9(1)

[a] Present calculated and experimental values are compared with the literature values.[26]

Table 3. Detected Raman-Active Modes for the LP Phase of $LiNiPO_4$ and Comparison with Calculations

	Theory			Experiments			Literature[30]
Mode symmetry	ω_0 (cm^{-1})	a (cm^{-1} GPa^{-1})	a (cm^{-1} GPa^{-2})	ω_0 (cm^{-1})	a (cm^{-1} GPa^{-1})	a (cm^{-1} GPa^{-2})	ω_0 (cm^{-1})
A_g	108.3	1.99	−0.023				114
B_{3g}	115.7	1.40	−0.017	120.8(2)	1.71(1)	−0.035(6)	122
B_{2g}	162.5	1.81	−0.027	170.3(2)	1.99(10)	−0.047(8)	172
A_g	168.7	1.58	−0.019	176.2(2)	1.65(8)	−0.031(7)	175.5
B_{1g}	168.9	4.21	−0.080				
B_{2g}	173.5	2.55	−0.027	182*			182
B_{3g}	185.8	3.51	−0.025				193.5
B_{1g}	188.6	2.37	0.009				199
A_g	227.6	3.23	−0.039	238.6(3)	3.74(13)	−0.09(1)	242.5
B_{2g}	243.0	2.96	−0.027				255.5
B_{1g}	245.3	4.10	−0.063				258
B_{3g}	247.1	3.79	−0.031	258.4(4)	4.07(20)	−0.102(17)	262
A_g	267.5	4.66	−0.061	283.3(3)	5.33(13)	−0.12(1)	287.5
A_g	291.0	3.87	−0.034	304.1(2)	4.77(8)	−0.109(7)	308
B_{2g}	294.0	3.04	−0.028				313
B_{1g}	304.5	4.05	−0.064				325
B_{3g}	310.2	3.79	−0.058				329
B_{2g}	310.2	5.34	−0.051	325.4(4)	4.27(17)	−0.103(14)	329.5
$B_{1g}(\nu_2)$	394.1	4.11	−0.003	417.6(3)	10.74(41)	−1.88(12)	422.5
$B_{3g}(\nu_2)$	412.8	5.53	−0.017	436.9(6)	6.65(67)	−0.36(14)	442.5
$A_g(\nu_2)$	437.6	3.78	−0.022	465.5(5)	2.78(26)	−0.006(21)	470.5
$B_{2g}(\nu_2)$	446.4	2.85	−0.018				470.5
$A_g(\nu_4)$	548.4	1.44	−0.004	581.5(4)	0.80(16)	−0.025(14)	581.5
$B_{3g}(\nu_4)$	556.2	2.00	−0.011	591.1(4)	1.59(16)	−0.003(13)	592
$B_{1g}(\nu_4)$	556.7	1.76	−0.009				592.5
$B_{2g}(\nu_4)$	565.7	1.82	−0.002	600(2)	−1(3)	−0.57(80)	603
$A_g(\nu_4)$	603.2	3.09	−0.016	640.4(3)	3.26(12)	−0.037(1)	642
$B_{2g}(\nu_4)$	617.5	3.27	−0.024	650*			

$A_g(\nu_1)$	890.7	3.28	−0.022	947.9(2)	3.58(9)	−0.054(8)	948.5
$B_{2g}(\nu_1)$	891.1	3.33	−0.023				
$B_{3g}(\nu_3)$	903.6	3.56	−0.023				953
$B_{1g}(\nu_3)$	933.2	3.30	−0.022	982*			986
$A_g(\nu_3)$	960.4	3.38	−0.028	1010.1(2)	3.87(11)	−0.088(9)	1011.5
$B_{2g}(\nu_3)$	971.4	3.34	−0.028	1021.2(5)	3.90(21)	−0.105(17)	1023
$A_g(\nu_3)$	1020.1	4.92	−0.034	1071.4(3)	5.60(14)	−0.095(11)	1074.5
$B_{2g}(\nu_3)$	1034.6	4.79	−0.033	1086.4(6)	5.8(3)	−0.12(2)	1090

[a] The symmetry of each mode is also reported, together with the parameters for the quadratic fit for the frequency $\omega(P) = \omega_0 + aP + bP^2$. The asterisks denote the modes that were detected only under ambient conditions. The uncertainties for the values obtained from the fits are reported as well, in the parentheses notation.

Table 4. Raman Modes of the β-Phase of LiNiPO4 with Their Predicted Symmetry and Coefficients of the Quadratic *Fit* $\omega = \omega_0 + aP + bP^2$ of Their Pressure Evolution[a]

	Theory			Experiments		
Mode symmetry	ω_{theo} (cm^{-1})	a (cm^{-1} GPa^{-1})	b (cm^{-1} GPa^{-2})	ω_{exp} (cm^{-1})	a (cm^{-1} GPa^{-1})	b (cm^{-1} GPa^{-2})
B_{3g}	143.1	−0.16	−0.008			
B_{1g}	174.0	0.86	−0.012	185*		
B_{1g}	238.6	1.73	−0.008			
A_g	240.8	2.68	−0.036	249.9(7)	2.80(21)	−0.059(14)
B_{1g}	247.9	2.54	−0.025	259*		
B_{2g}	282.9	3.73	−0.005			
B_{3g}	344.7	2.62	−0.008	343*		
A_g	367.9	2.88	−0.011			
B_{2g}	426.1	2.54	0.002	444*		
A_g	436.3	1.92	0.003	453.8(6)	1.98(20)	0.003(13)
B_{3g}	500.6	2.38	−0.012	497*		
B_{1g}	528.4	0.72	0.001	565.0(6)	0.66(17)	0.002(11)
A_g	595.3	3.22	−0.028	619(1)	3.20(41)	−0.033(27)
B_{3g}	614.8	3.47	−0.001	646.7(8)	3.59(36)	−0.001(34)
B_{1g}	851.4	5.01	−0.029	912(2)	5.09(51)	−0.039(33)
A_g	877.9	4.76	−0.008	940.7(6)	4.70(19)	−0.018(12)
A_g	1002.4	4.52	−0.023	1057.5(9)	4.40(28)	−0.032(18)
B_{3g}	1094.1	4.96	−0.033	1147.4(8)	4.84(24)	−0.041(16)
B_{1g}	238.6	1.73	−0.008			
A_g	240.8	2.68	−0.036	249.9(7)	2.80(21)	−0.059(14)

[a] ω_{theo} represents the modes calculated from first-principles, while ω_{exp} represents the actually observed modes. Missing modes could not be observed or followed because they were either too weak or lie outside the experimental range. The asterisks denote the modes that can be measured only under ambient conditions. The uncertainties for the values obtained from the fits are reported as well (in the parentheses notation).

Table 5. Atomic Coordinates for β-$LiNiPO_4$ at Ambient Pressure, Space Group Cmcm (No. 63); Comparison between Calculated Values and the Literature Values[13]

		Calculated			Literature		
atom	site	x/a	y/b	z/c	x/a	y/b	z/c
Li	4c	0	0.67129	1/4	0	0.672(2)	1/4
Ni	4a	0	0	0	0	0	0
P	4c	0	0.34894	1/4	0	0.3504(3)	1/4
O(1)	8f	0	0.24401	0.04555	0	0.246(3)	0.044(1)
O(2)	8g	0.23176	0.46713	1/4	0.227(1)	0.466(3)	1/4

Table 6. Lattice Parameters for β-$LiNiPO_4$ at Ambient Pressure, Space Group Cmcm (No. 63); Present Calculated and Experimental Values Are Compared with the Literature Values[13]

parameter	calculated	experimental	literature
a (Å)	5.4094	5.358(1)	5.3580(2)
b (Å)	8.2023	8.127(1)	8.1272(3)
c (Å)	6.1933	6.124(1)	6.1241(3)
volume ($Å^3$)	274.79	266.7(2)	266.7(1)

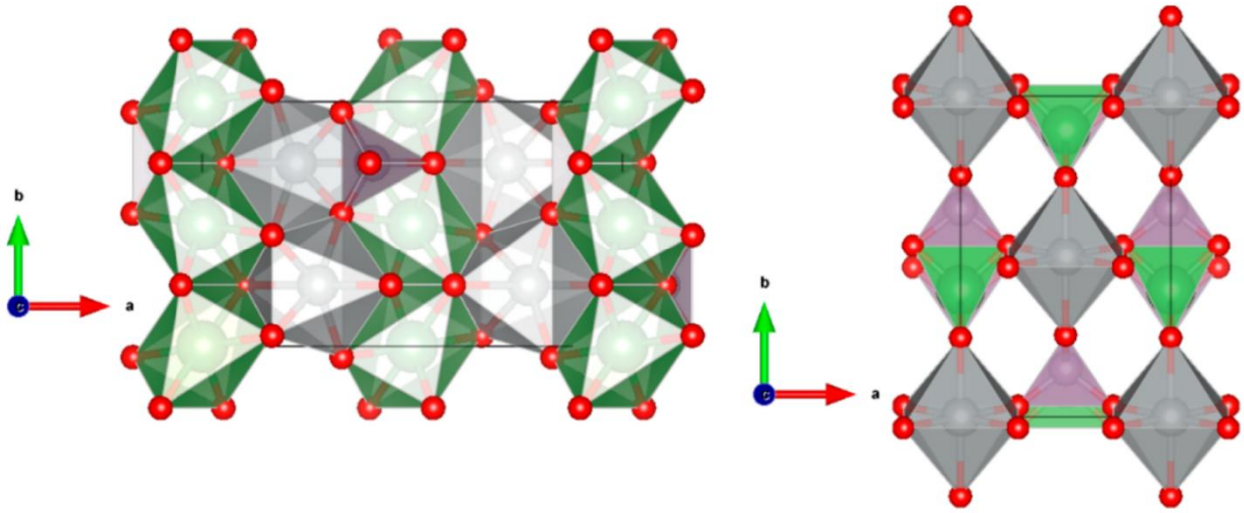

Figure 1. Schematic representation of the olivine phase (α-phase) of $LiNiPO_4$ (left) and the high-pressure Na_2CrO_4 phase (β-phase) of $LiNiPO_4$ (right). Li coordination polyhedra are shown in green, Ni coordination polyhedra are shown in gray, and P coordination polyhedra are shown in purple.

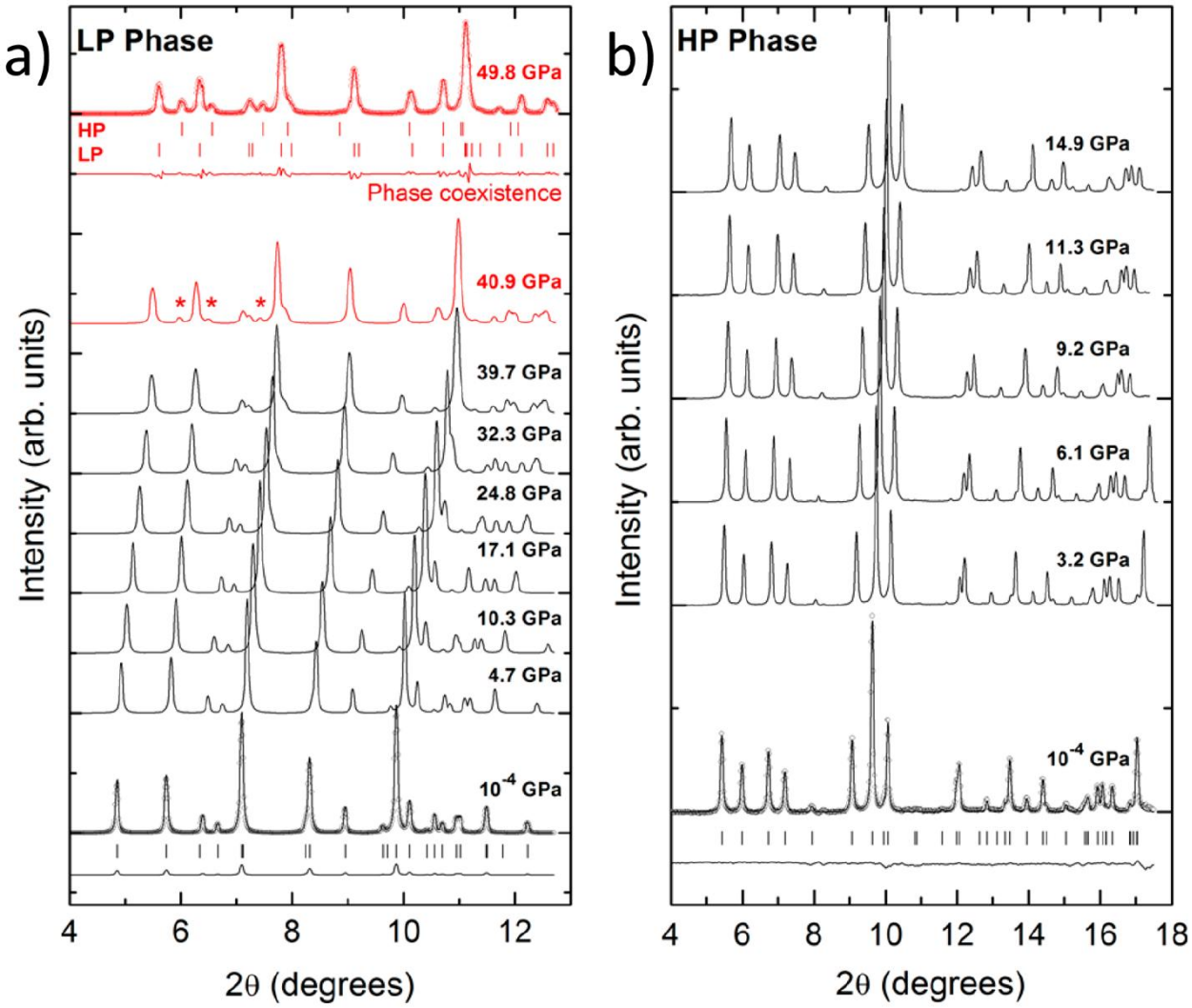

Figure 2. (a) XRD patterns of α-$LiNiPO_4$ at selected pressures. Rietveld refinements are only shown for the patterns at ambient pressure (10^{-4} GPa) and at 49.8 GPa. For the fitted diffractograms, the experimental data are represented by open circles, Rietveld refinements and residuals are shown as solid lines. Vertical ticks indicate the position of the Bragg reflections. LP and HP indicate the position of the peaks for the α and the incipient β phase, respectively. (b) XRD patterns for the synthesized β-LiNiPO4 at selected pressures. Rietveld refinement is only shown for patternat ambient pressure (10^{-4} GPa); experimental data for the refined pattern are represented by open circles, while the Rietveld refinement and the residuals are shown as solid lines. Vertical ticks indicate the positions of the Bragg reflections.

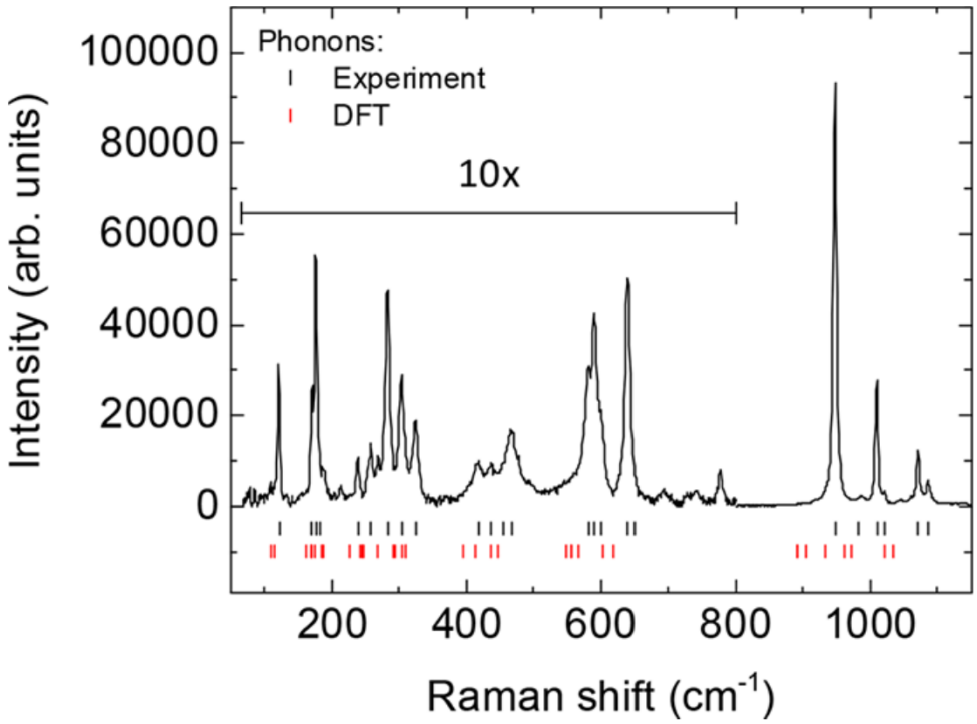

Figure 3. Raman spectrum of olivine-type LiNiPO4 at ambient pressure (black line). Experimentally detected modes (black ticks). Theoretical modes (red ticks). For spatial frequencies below 800 cm^{-1}, the vertical scale has been magnified by a factor of 10, to increase the readability of the spectrum. Weak modes around 700−800 cm^{-1} and near 1050 cm^{-1} are associated with overtones.[30]

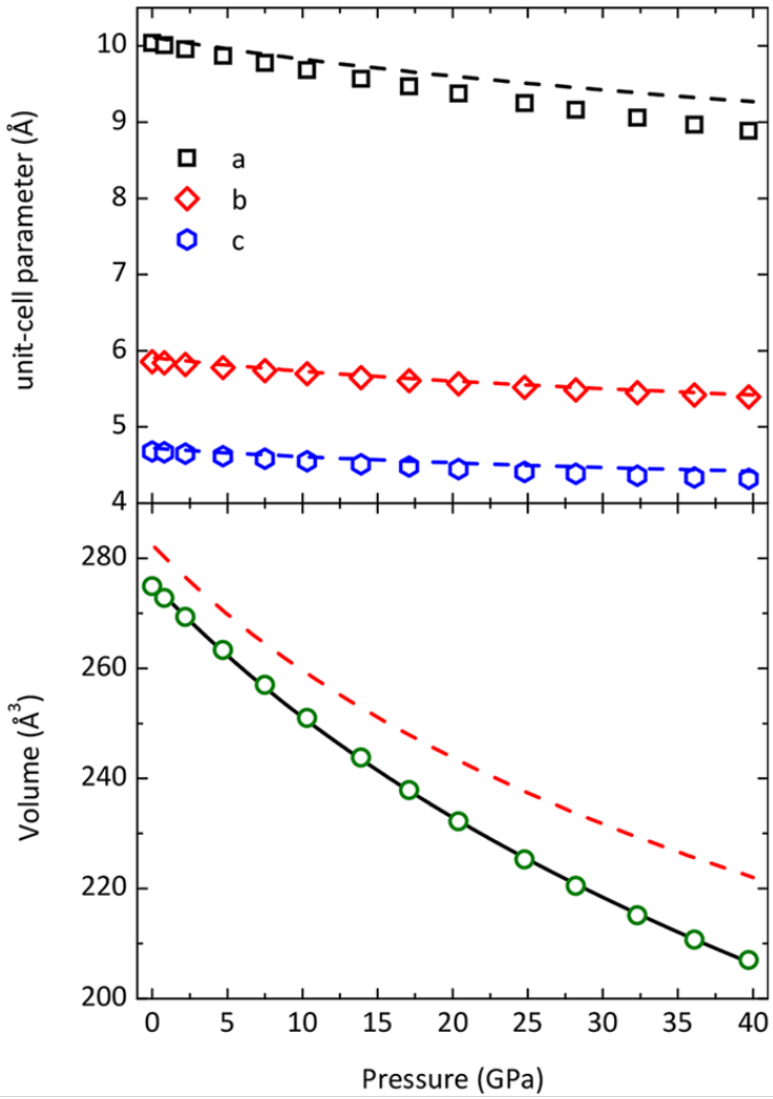

Figure 4. Pressure dependence of the unit-cell parameters for α-$LiNiPO_4$, up to 39.7 GPa. Open symbols represent experimental data, dashed lines represent theoretical calculations (GGA+U DFT), and the black continuous line is the third-order Birch−Murnaghan equation of state (EOS) fit for the pressure−volume data.

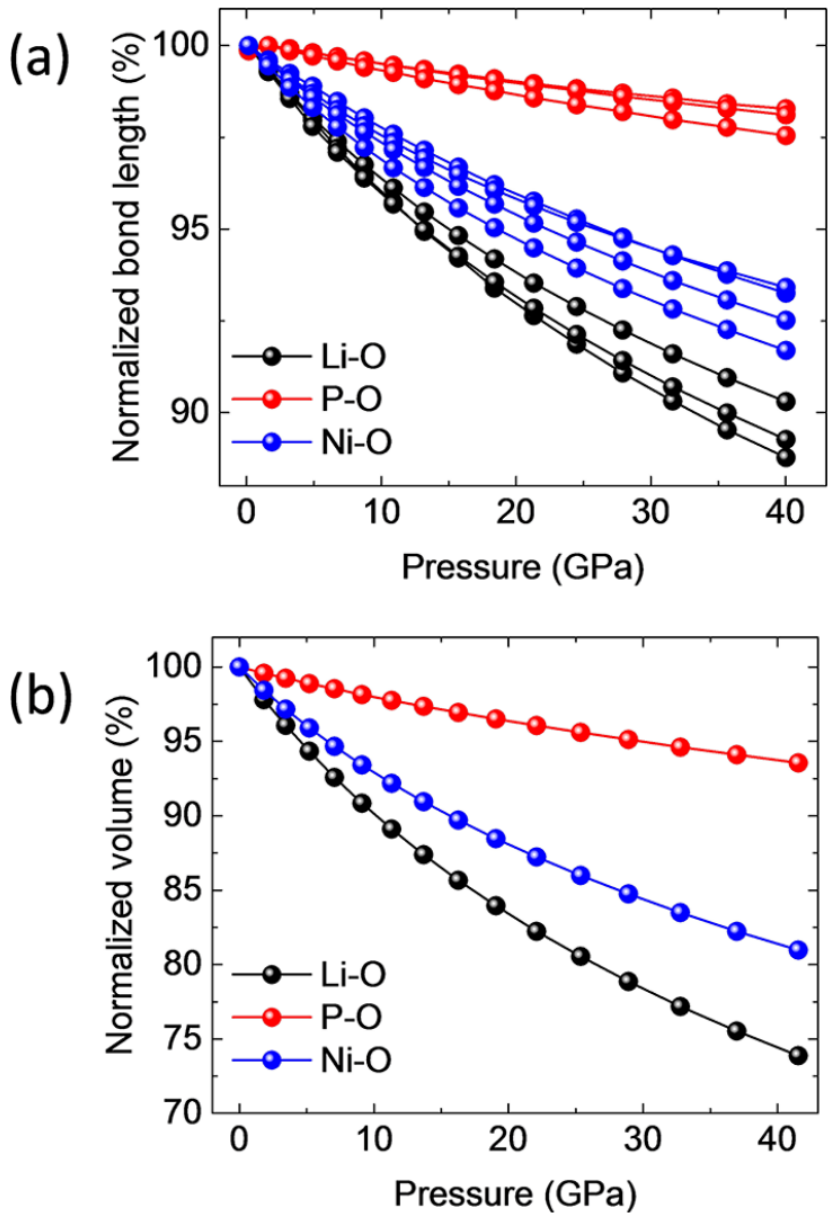

Figure 5. (a) Normalized contraction of the atomic bonds in LiO_6, PO_4, and NiO_6 polyhedra, calculated according to GGA+U. (b) Normalized volume change of the aforementioned polyhedra under compression.

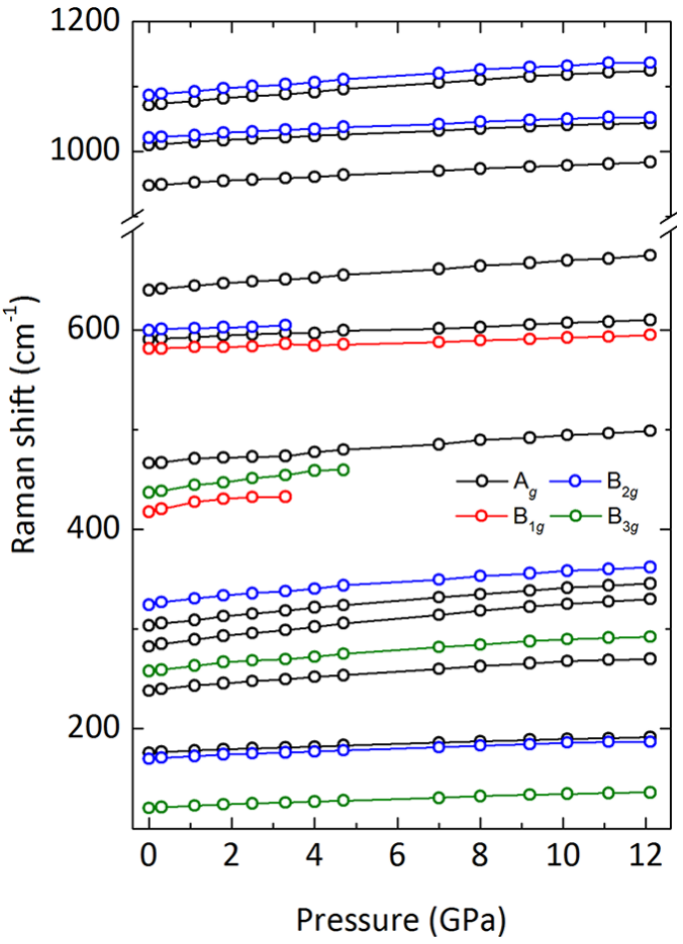

Figure 6. Evolution of the experimentally detected Raman modes of the olivine phase with pressure. The symmetry of each mode is also shown. Lines are present to serve as guides to the eye.

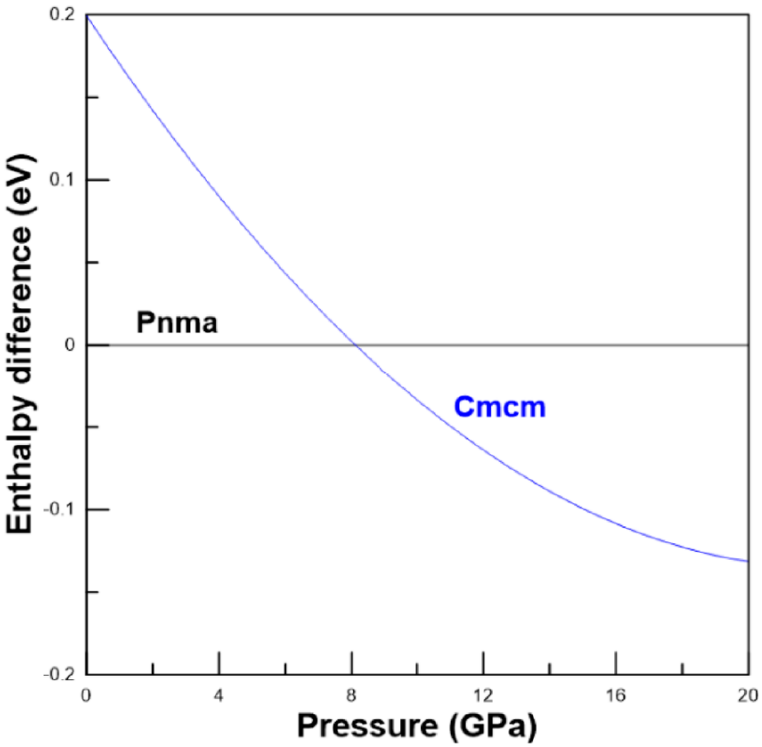

Figure 7. Enthalpy difference versus pressure for the LP (Pnma) and HP (Cmcm) phases of Li $NiPO_4$.

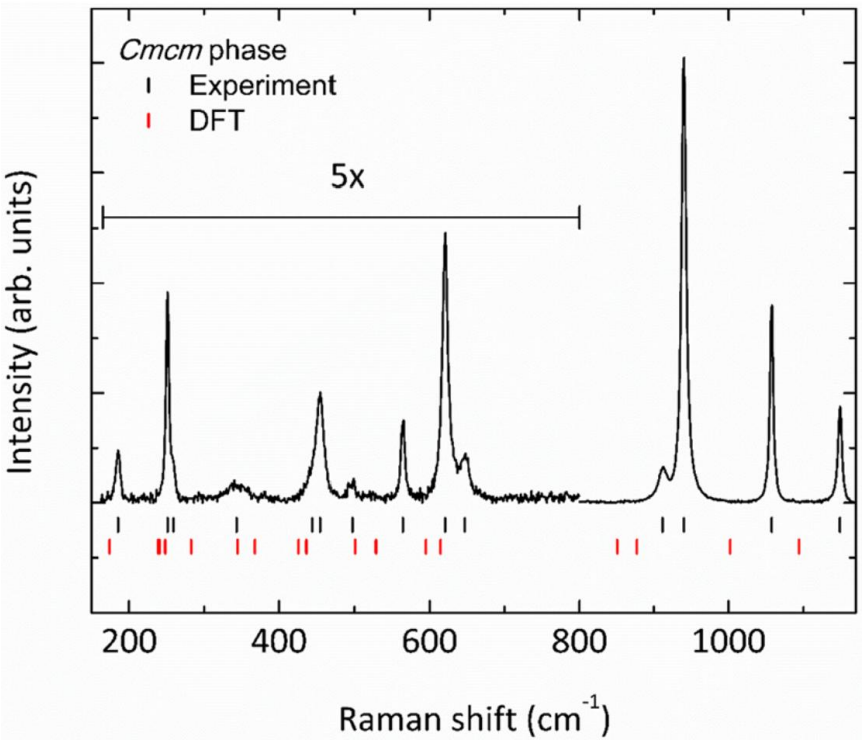

Figure 8. Raman spectrum of the synthesized β-phase of $LiNiPO_4$. Predicted phonons (DFT) are marked in red. There is one mode predicted at 143.1 cm^{-1} that is not seen in the figure, because it is outside the frequency range of the experiment. Experimentally detected phonons are marked in black. As in the case of the α- phase, calculated phonons are nonuniformly shifted, with respect to the experimentally detected phonons.

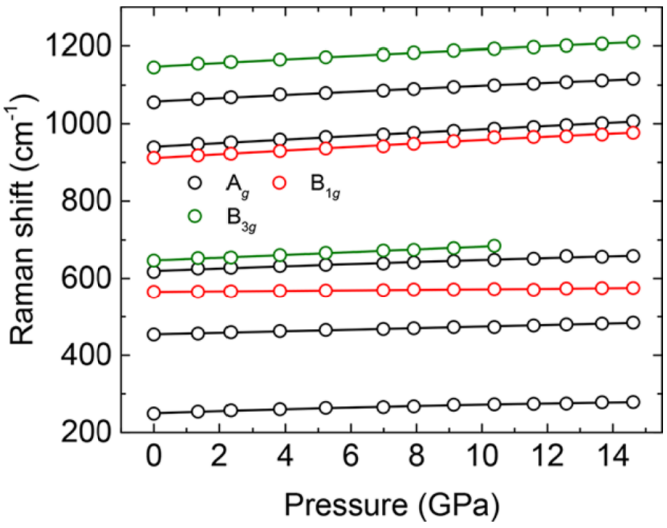

Figure 9. Evolution of Raman modes for the β-phase of $LiNiPO_4$ (Cmcm space group). Lines are the quadratic fit $\omega = \omega_0 + aP + bP^2$.

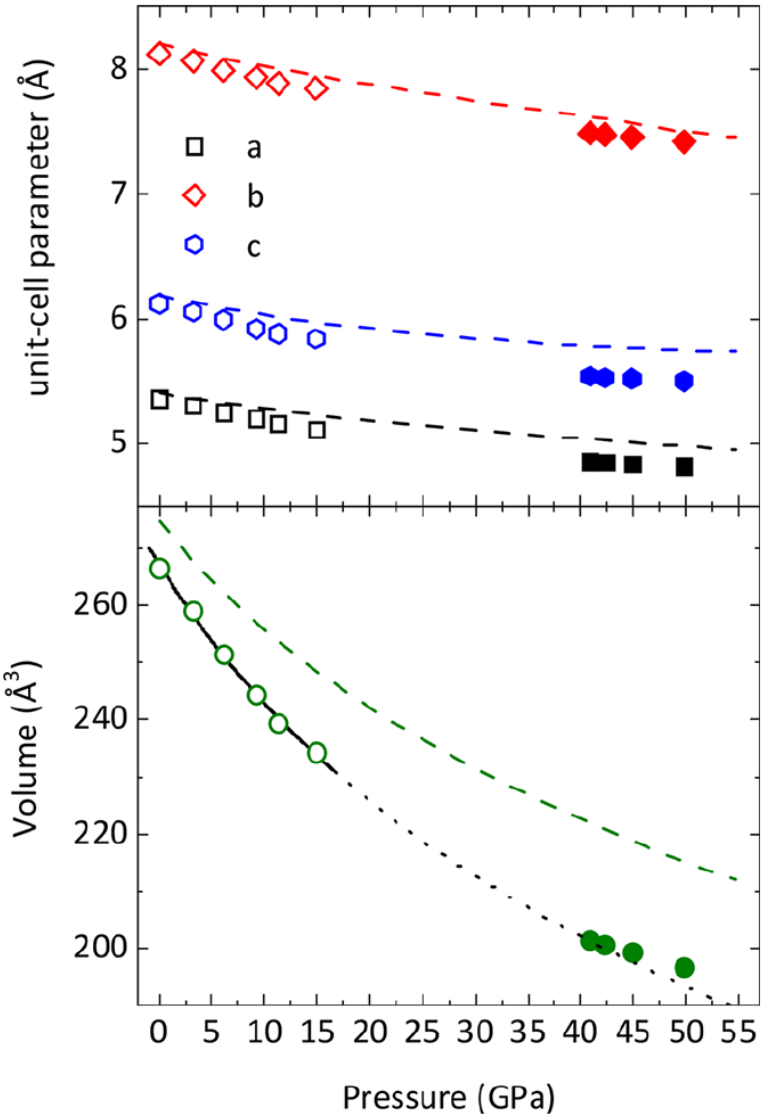

Figure 10. Pressure dependence of the cell parameters and cell volume for the synthesized β-phase of $LiNiPO_4$, up to 14.9 GPa. Open symbols represent experimental data. Dashed lines represent ab initio calculations (DFT). The black continuous line represents the third-order Birch−Murnaghan EOS fit. The dotted black line represents the extrapolation of the EOS fit beyond 14.9 GPa. Closed symbols in the high-pressure range (P > 50 GPa) are the data obtained for the emerging β-phase observed at high pressure and RT. These have been obtained by Rietveld refinements of the XRD patterns in Figure S1 for P > 40 GPa (coexistence region), considered as the superposition of two distinct phases (high-pressure α-phase and incipient β-phase).

References

(1) Padhi, A. of K. ALBA Phospho-Olivines staff. as Positive-Electrode Materials for Rechargeable Lithium Batteries. J. Electrochem. Soc. 1997, 144, 1188.
(2) Howard, W. F.; Spotnitz, R. M. Theoretical Evaluation of High- Energy Lithium Metal Phosphate Cathode Materials in Li-Ion Batteries. J. Power Sources 2007, 165, 887−891.
(3) Minakshi, M.; Ralph, D.; Blackford, M.; Ionescu, M. $LiNiPO_4$ Aqueous Rechargeable Battery. ECS Trans. 2011, 35, 281−292.
(4) Lacomba-Perales, R.; Errandonea, D.; Meng, Y.; Bettinelli, M. High-Pressure Stability and Compressibility of APO_4 (A = La, Nd, Eu, Gd, Er, and Y) Orthophosphates: An x-Ray Diffraction Study Using Synchrotron Radiation. Phys. Rev. B: Condens. Matter Mater. Phys. 2010, 81, 064113. (5) Gomis, O.; Lavina, B.; Rodríguez-Hernández, P.; Muñoz, A.; Errandonea, R.; Errandonea, D.; Bettinelli, M. High-Pressure Structural, Elastic, and Thermodynamic Properties of Zircon-Type $HoPO_4$ and $TmPO_4$. J. Phys.: Condens. Matter 2017, 29, 095401.
(6) Errandonea, D.; Gomis, O.; Rodríguez-Hernández, P.; Muñoz, A.; Ruiz-Fuertes, J.; Gupta, M.; Achary, S. N.; Hirsch, A.; Manjon, F. J.; Peters, L.; et al. High-Pressure Structural and Vibrational
Properties of Monazite-Type $BiPO_4$, $LaPO_4$, $CePO_4$, and $PrPO_4$. J. Phys.: Condens. Matter 2018, 30, 065401.
(7) Ashton, T. E.; Laveda, J. V.; MacLaren, D. A.; Baker, P. J.; Porch, A.; Jones, M. O.; Corr, S. A. Muon Studies of Li^+ Diffusion in $LiFePO_4$ Nanoparticles of Different Polymorphs. J. Mater. Chem. A 2014, 2, 6238−6245.
(8) Islam, M. M.; Bredow, T. Lithium Diffusion Pathways in β-Li2TiO3: A Theoretical Study. J. Phys. Chem. C 2016, 120, 7061−7066.
(9) Núñez-Valdez, M. N.; Efthimiopoulos, I.; Taran, M.; McCammon, C.; Mü ller, J.; Bykova, E.; Koch-Müller, M.; Wilke, M. Evidence for a Pressure-Induced Spin Transition in Olivine-Type
LiFePO4 Triphylite. Phys. Rev. B: Condens. Matter Mater. Phys. 2018, 97, 184405.
(10) Binns, R. A.; Davis, R. J.; Reed, S. J. B. Ringwoodite, Natural (Mg,Fe)2SiO4 Spinel in the Tenham Meteorite. Nature 1969, 221, 943−944.
(11) Arroyo-de Dompablo, M. E.; Amador, U.; Alvarez, M.; Gallardo, J. M.; García-Alvarado, F. Novel Olivine and Spinel LiMAsO4 (M = 3d metal) as Positive Electrode Materials in Lithium
Cells. Solid State Ionics 2006, 177, 2625−2628.
(12) Alvarez-Vega, M.; Gallardo-Amores, J. M.; García-Alvarado, F.; Amador, U. Synthesis and Structure of Olivine-like Arsenates (M = Mn, Fe, Co and Ni) and Their High-Pressure Spinel-like Polymorphs. Solid State Sci. 2006, 8, 952−957.
(13) Amador, U.; Gallardo-Amores, J. M.; Heymann, G.; Huppertz, H.; Morá n, E.; Arroyo y de Dompablo, M. E. High Pressure Polymorphs of LiCoPO4 and LiCoAsO4. Solid State Sci. 2009, 11, 343−348.
(14) García-Moreno, O.; Alvarez-Vega, M.; García-Jaca, J.; Gallardo- Amores, J. M.; Sanjuán, M. L.; Amador, U. Influence of the Structure on the Electrochemical Performance of Lithium Transition Metal Phosphates as Cathodic Materials in Rechargeable Lithium Batteries: A New High-Pressure Form of LiMPO4 (M = Fe and Ni). Chem. Mater. 2001, 13, 1570−1576.
(15) Dewaele, A.; Torrent, M.; Loubeyre, P.; Mezouar, M. Compression Curves of Transition Metals in the Mbar Range: Experiments and Projector Augmented-Wave Calculations. Phys. Rev. B: Condens. Matter Mater. Phys. 2008, 78, 1−13.
(16) Fauth, F.; Peral, I.; Popescu, C.; Knapp, M. The New Material Science Powder Diffraction Beamline at ALBA Synchrotron. Powder Diffr. 2013, 28, S360−S370.
(17) Kraus, W.; Nolze, G. POWDER CELL□A Program for the Representation and Manipulation of Crystal Structures and Calculation of the Resulting X-Ray Powder Patterns. J. Appl. Crystallogr. 1996, 29, 301−303.

(18) Hohenberg, P.; Kohn, W. Inhomogeneous Electron Gas. Phys. Rev. 1964, 136, B864−B871.
(19) Kresse, G.; Furthmü ller, J. Efficient Iterative Schemes for Ab Initio Total-Energy Calculations Using a Plane-Wave Basis Set. Phys. Rev. B: Condens. Matter Mater. Phys. 1996, 54, 11169−11186.
(20) Kresse, G.; Joubert, D. From Ultrasoft Pseudopotentials to theProjector Augmented-Wave Method. Phys. Rev. B: Condens. MatterMater. Phys. 1999, 59, 1758−1775.
(21) Blöchl, P. E. Projector Augmented-Wave Method. Phys. Rev. B: Condens. Matter Mater. Phys. 1994, 50, 17953−17979.
(22) Perdew, J. P.; Burke, K.; Ernzerhof, M. Generalized GradientApproximation Made Simple. Phys. Rev. Lett. 1996, 77, 3865−3868.
(23) Dudarev, S. L.; Botton, G. A.; Savrasov, S. Y.; Humphreys, C. J.;Sutton, A. P. Electron-Energy-Loss Spectra and the Structural Stability of Nickel Oxide: An LSDA+U Study. Phys. Rev. B: Condens. Matter Mater. Phys. 1998, 57, 1505−1509.
(24) Shang, S. L.; Wang, Y.; Mei, Z. G.; Hui, X. D.; Liu, Z. K. Lattice Dynamics, Thermodynamics, and Bonding Strength of Lithium-Ion Battery Materials LiMPO4 (M = Mn, Fe, Co, and Ni): A Comparative First-Principles Study. J. Mater. Chem. 2012, 22, 1142−1149.
(25) Parlinski, K. Computer Code PHONON; available via the Internet at: http://wolf.ifj.edu.pl/phonon/.
(26) Julien, C. M.; Mauger, A.; Zaghib, K.; Veillette, R.; Groult, H. Structural and Electronic Properties of the LiNiPO4 Orthophosphate. Ionics 2012, 18, 625−633.
(27) Warda, S. A.; Lee, S.-L. Refinement of the Crystal Structure of Lithium Nickel Phosphate, LiNiPO4. Z. Kristallogr.– New Cryst. Struct. 1997, 212, 319.
(28) Salah, A. A.; Jozwiak, P.; Garbarczyk, J.; Benkhouja, K.; Zaghib, K.; Gendron, F.; Julien, C. M. Local Structure and Redox Energies of Lithium Phosphates with Olivine- and Nasicon-like Structures. J. Power Sources 2005, 140, 370−375.
(29) Ramana, C. V.; Ait-Salah, A.; Utsunomiya, S.; Becker, U.; Mauger, A.; Gendron, F.; Julien, C. M. Structural Characteristics of Lithium Nickel Phosphate Studied Using Analytical Electron Microscopy and Raman Spectroscopy. Chem. Mater. 2006, 18, 3788−3794.
(30) Errandonea, D.; Muñoz, A.; Rodríguez-Hernández, P.; Proctor, J. E.; Sapiña, F.; Bettinelli, M. Theoretical and Experimental Study of the Crystal Structures, Lattice Vibrations, and Band Structures of Monazite-Type PbCrO4, PbSeO4, SrCrO4, and SrSeO4. Inorg. Chem. 2015, 54, 7524−7535.
(31) Fomin, V. I.; Gnezdilov, V. P.; Kurnosov, V. S.; Peschanskii, A.V.; Yeremenko, A. V.; Schmid, H.; Rivera, J. P.; Gentil, S. Raman Scattering in LiNiPO4 Single Crystal. Low Temp. Phys. 2002, 28, 203.(32) Frost, R. L.; Williams, P. A.; Martens, W.; Kloprogge, J. T.; Leverett, P. Raman Spectroscopy of the Basic Copper Phosphate Minerals Cornetite, Libethenite, Pseudomalachite, Reichenbachite and Ludjibaite. J. Raman Spectrosc. 2002, 33, 260−263.
(33) Errandonea, D.; Muñ oz, A.; Gonzalez-Platas, J. Comment on High-Pressure x-Ray Diffraction Study of YBO3/Eu3+, GdBO3, and EuBO3: Pressure-Induced Amorphization in GdBO3. J. Appl. Phys. 2014, 115, 1−4.
(34) Dong, H.; Guo, H.; He, Y.; Gao, J.; Han, W.; Lu, X.; Yan, S.; Yang, K.; Li, H.; Chen, D.; et al. Structural Stability and Li-Ion Transport Property of LiFePO4 under High-Pressure. Solid State
Ionics 2017, 301, 133−137.
(35) Errandonea, D.; Muñoz, A.; Rodríguez-Herná ndez, P.; Gomis, O.; Achary, S. N.; Popescu, C.; Patwe, S. J.; Tyagi, A. K. High-Pressure Crystal Structure, Lattice Vibrations, and Band Structure of BiSbO4. Inorg. Chem. 2016, 55, 4958−4969.
(36) Errandonea, D.; Gomis, O.; Santamaría-Perez, D.; García-Domene, B.; Muñoz, A.; Rodríguez-Hernández, P.; Achary, S. N.; Tyagi, A. K.; Popescu, C. Exploring the High-Pressure Behavior of the Three Known Polymorphs of BiPO4: Discovery of a New Polymorph. J. Appl. Phys. 2015, 117, 105902.

(37) Birch, F. Finite Strain Isotherm and Velocities for Single-Crystal and Polycrystalline NaCl at High Pressures and 300 K. J. Geophys. Res. 1978, 83, 1257.
(38) Andrault, D.; Bouhifd, M. A.; Itie, J. P.; Richet, P. Compression and Amorphization of (Mg,Fe)2SiO4 Olivines: An X-Ray Diffraction Study up to 10 GPa. Phys. Chem. Miner. 1995, 22, 99−107.
(39) Yagi, T.; Ida, Y.; Sato, Y.; Akimoto, S.-I. Effect of Hydrostatic Pressure on the Lattice Parameters of Fe2SiO4 Olivine up to 70 Kbar. Phys. Earth Planet. Inter. 1975, 10, 348−354.
(40) Liu, Q.; Liu, W.; Whitaker, M.; Wang, L.; Li, B. Compressional and Shear Wave Velocities of Fe2SiO4 Spinel at High Pressure and High Temperature. High Pressure Res. 2008, 28, 405−413.
(41) Bass, J. D.; Weidner, D. J.; Hamaya, N.; Ozima, M.; Akimoto, S. Elasticity of the Olivine and Spinel Polymorphs of Ni2SiO4. Phys. Chem. Miner. 1984, 10, 261−272.
(42) Hazen, R. M.; Downs, R. T.; Finger, L. W. High-Pressure Crystal Chemistry of LiScSiO4 ; an Olivine with Nearly Isotropic Compression. Am. Mineral. 1996, 81, 327−334.
(43) Errandonea, D.; Ferrer-Roca, C.; Martínez-Garcia, D.; Segura, A.; Gomis, O.; Muñoz, A.; Rodríguez-Herná ndez, P.; López-Solano, J.; Alconchel, S.; Sapiña, F. High-Pressure X-Ray Diffraction and Ab Initio Study of Ni 2MoN, Pd2MoN, Pt2 Mo 3 N, Co3Mo3N, and Fe3Mo3N: Two Families of Ultra-Incompressible Bimetallic Inter- stitial Nitrides. Phys. Rev. B: Condens. Matter Mater. Phys. 2010, 82, 174105.
(44) Pellicer-Porres, J.; Saitta, A. M.; Polian, A.; Itié , J. P.; Hanfland,M. Six-Fold-Coordinated Phosphorus by Oxygen in AlPO4 Quartz Homeotype under High Pressure. Nat. Mater. 2007, 6, 698−702.
(45) Zurek, E.; Grochala, W. Predicting Crystal Structures and Properties of Matter under Extreme Conditions via Quantum Mechanics: The Pressure Is On. Phys. Chem. Chem. Phys. 2015, 17,
2917−2934.
(46) Garg, A. B.; Errandonea, D.; Popescu, C.; Martinez-García, D.; Pellicer-Porres, J.; Rodríguez-Herná ndez, P.; Muñoz, A.; Botella, P.; Cuenca-Gotor, V. P.; Sans, J. A. Pressure-Driven Isostructural Phase Transition in InNbO 4: In Situ Experimental and Theoretical Investigations. Inorg. Chem. 2017, 56, 5420−5430.
(47) Grimvall, G.; Magyari-Köpe, B.; Ozoliņs, E. N. M.; Persson, K. A. Lattice Instabilities in Metallic Elements. Rev. Mod. Phys. 2012, 84, 945−986.
(48) Garg, A. B.; Errandonea, D.; Rodríguez-Herná ndez, P.; López- Moreno, S.; Muñ oz, A.; Popescu, C. High-Pressure Structural Behaviour of HoVO4: Combined XRD Experiments and Ab Initio Calculations. J. Phys.: Condens. Matter 2014, 26, 265402.
(49) Schierz, P.; Zierenberg, J.; Janke, W. First-Order Phase Transitions in the Real Microcanonical Ensemble. Phys. Rev. E: Stat. Phys., Plasmas, Fluids, Relat. Interdiscip. Top. 2016, 94, 1−5.
(50) Errandonea, D.; Pellicer-Porres, J.; Pujol, M. C.; Carvajal, J. J.; Aguiló, M. Room-temperature vibrational properties of potassium gadolinium double tungstate under compression up to 32 GPa. J. Alloys Compd. 2015, 638, 14−20.
(51) Angel, R. J. Equations of State. Rev. Mineral. Geochem. 2000, 41, 35−59.
(52) Ringwood, A. E. The Olivine−Spinel Transition in the Earth's Mantle. Nature 1956, 178, 1303−1304.
(53) Maxisch, T.; Ceder, G. Elastic Properties of Olivine Lix FePO4 from First Principles. Phys. Rev. B: Condens. Matter Mater. Phys. 2006, 73, 174112.
(54) Hanic, F.; Handlović, M.; Burdová , K.; Majling, J. Crystal Structure of Lithium Magnesium Phosphate, LiMgPO4: Crystal Chemistry of the Olivine-Type Compounds. J. Crystallogr. Spectrosc. Res. 1982, 12, 99−127.
(55) Errandonea, D.; Garg, A. B. Recent Progress on the Characterization of the High-Pressure Behaviour of AVO4 Orthovanadates. Prog. Mater. Sci. 2018, 97, 123−169.

Effect of High Pressure on the Crystal Structure and Vibrational Properties of Olivine-type $LiNiPO_4$

-

Supporting Information

Enrico Bandiello[1],* Daniel Errandonea[1], Julio Pellicer-Porres[1], Alka B. Garg[2], Placida Rodriguez-Hernandez[3], Alfonso Muñoz[3], Domingo Martinez-Garcia[1], Rekha Rao[4], Catalin Popescu[5]

[1]*Departamento de Física Aplicada-ICMUV, MALTA Consolider Team, Universidad de Valencia, Edificio de Investigación, C/Dr. Moliner 50, Burjassot, 46100 Valencia, Spain*

[2]*High Pressure and Synchrotron Radiation Physics Division, Bhabha Atomic Research Centre, Mumbai, 400085, Maharashtra, India*

[3]*Departamento de Física, Instituto de Materiales y Nanotecnología, MALTA Consolider Team, Universidad de La Laguna, La Laguna, E-38205 Tenerife, Spain*

[4]*Solid State Physics Division, Bhabha Atomic Research Centre, Mumbai, 400085, India*

[5]*CELLS-ALBA Synchrotron Light Facility, Cerdanyola del Valles, 08290 Barcelona, Spain*

[*]Corresponding author: *enrico.bandiello@uv.es*

Mode Symmetry	ω_0 (cm^{-1})	a ($cm^{-1}\,GPa^{-1}$)	b ($cm^{-1}\,GPa^{-2}$)
B_{3u}	155.2	1.75	-0.026
B_{1u}	184.9	2.30	-0.047
B_{3u}	188.7	3.07	-0.039
B_{2u}	193.6	1.49	-0.028
B_{1u}	211.8	2.76	-0.032
B_{2u}	224.4	3.82	-0.094
B_{2u}	240.3	7.02	-0.074
B_{1u}	244.0	3.88	-0.053
B_{2u}	248.5	8.68	-0.136
B_{3u}	257.9	6.29	-0.113
B_{1u}	286.0	4.21	-0.0874
B_{3u}	292.3	5.97	-0.114
B_{1u}	297.3	6.89	-0.032
B_{3u}	317.7	4.30	0.007
B_{2u}	334.7	5.52	-0.004
B_{3u}	345.2	5.67	-0.015
B_{1u}	355.5	6.20	-0.062
B_{2u}	431.6	5.36	-0.062
B_{2u}	444.2	8.36	-0.206
B_{1u}	474.6	3.96	-0.012
B_{3u}	487.7	4.36	-0.064
B_{3u}	495.2	7.56	-0.165
B_{1u}	502.6	8.47	-0.216
$B_{2u}(\nu_4)$	511.1	2.32	0.151
$B_{3u}(\nu_4)$	540.8	3.16	0.098
$B_{1u}(\nu_4)$	545.0	3.07	0.076
$B_{1u}(\nu_4)$	607.3	2.67	0.037
$B_{3u}(\nu_4)$	619.8	2.98	-0.001
$B_{3u}(\nu_1)$	885.7	3.33	-0.023
$B_{1u}(\nu_1)$	887.3	3.30	-0.023
$B_{2u}(\nu_3)$	896.9	3.50	-0.021
$B_{3u}(\nu_3)$	977.4	3.48	-0.028
$B_{1u}(\nu_3)$	1020.3	4.89	-0.037
$B_{3u}(\nu_3)$	1045.5	4.79	-0.032
$B_{1u}(\nu_3)$	1087.9	3.56	-0.026

Table S1: Calculated IR modes for the LP phase of $LiNiPO_4$, with the coefficients of the pressure dependence. $\omega = \omega_0 + aP + bP^2$. The mode assignment is given. Different internal vibrations of the PO_4 tetrahedron are identified.

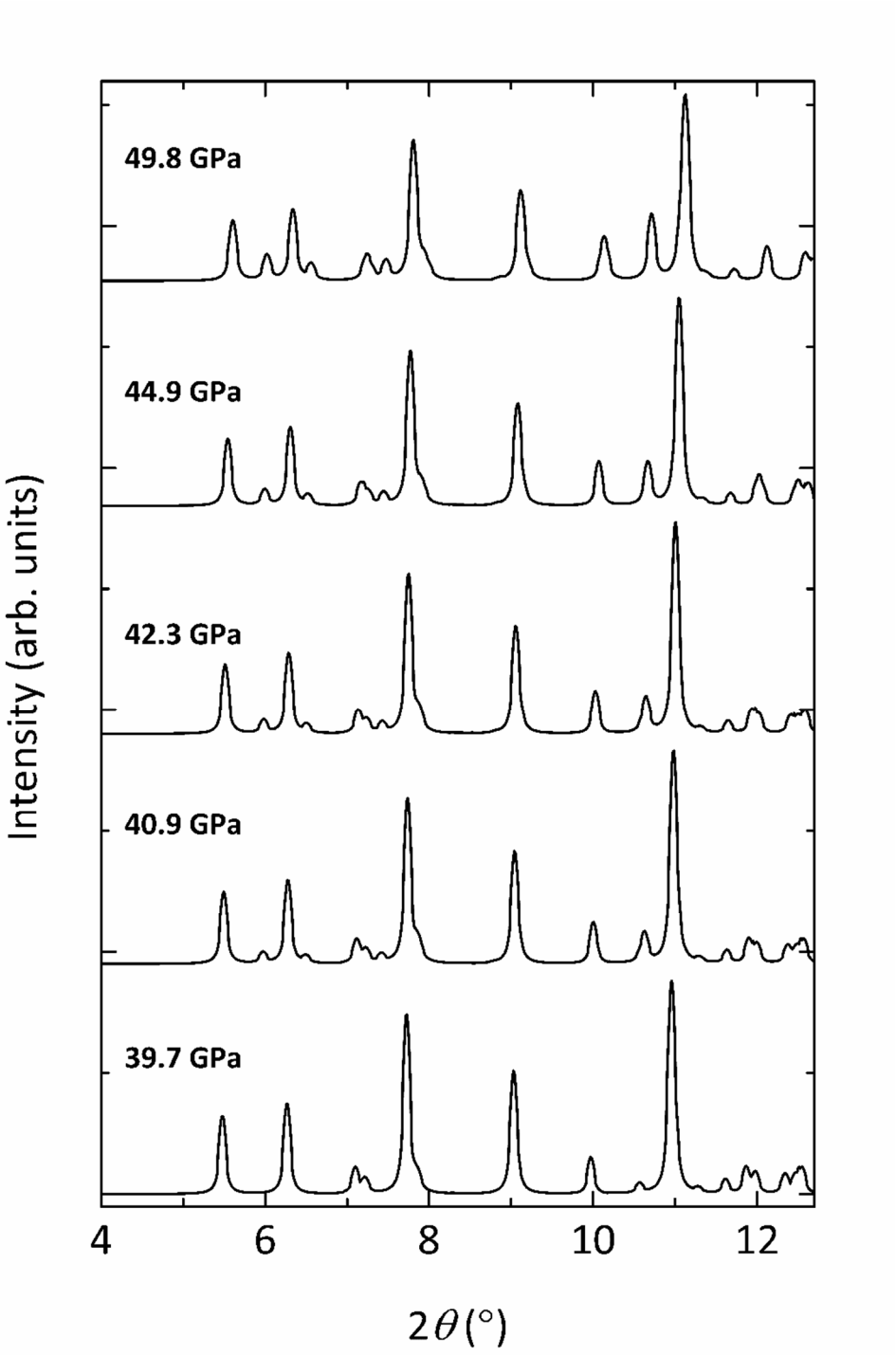

Figure S1. XRD patterns for $LiNiPO_4$ from 39.7 GPa to 49.8 GPa, with new Bragg reflections clearly appearing above 39.7 GPa.

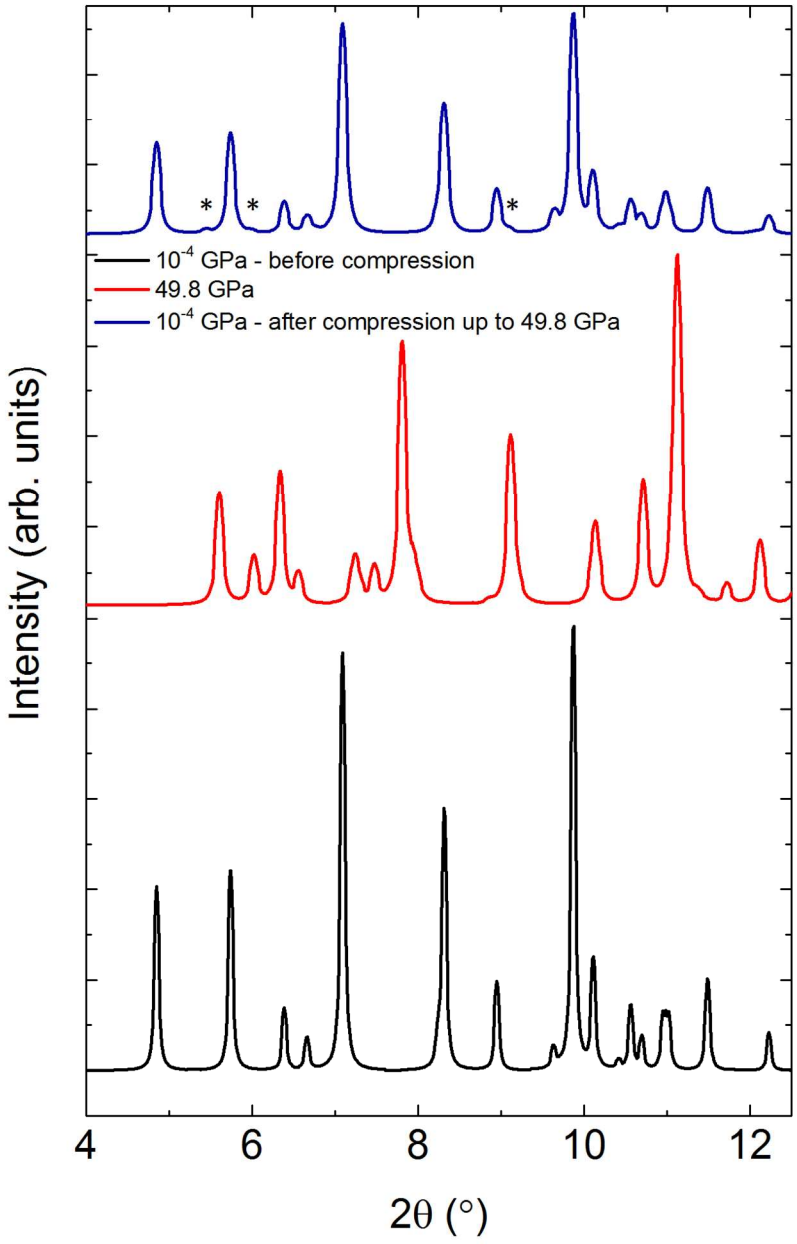

Figure S2. Comparison of the XRD patterns for $LiNiPO_4$ (for the initial α phase). Black: pattern at ambient pressure, red: pattern at 48.9 GPa and blue: pattern at ambient conditions after pressure release. The presence of minimal hysteresis can be appreciated by the weak peaks in the blue pattern (asterisks) and in the broadening of the original peaks.

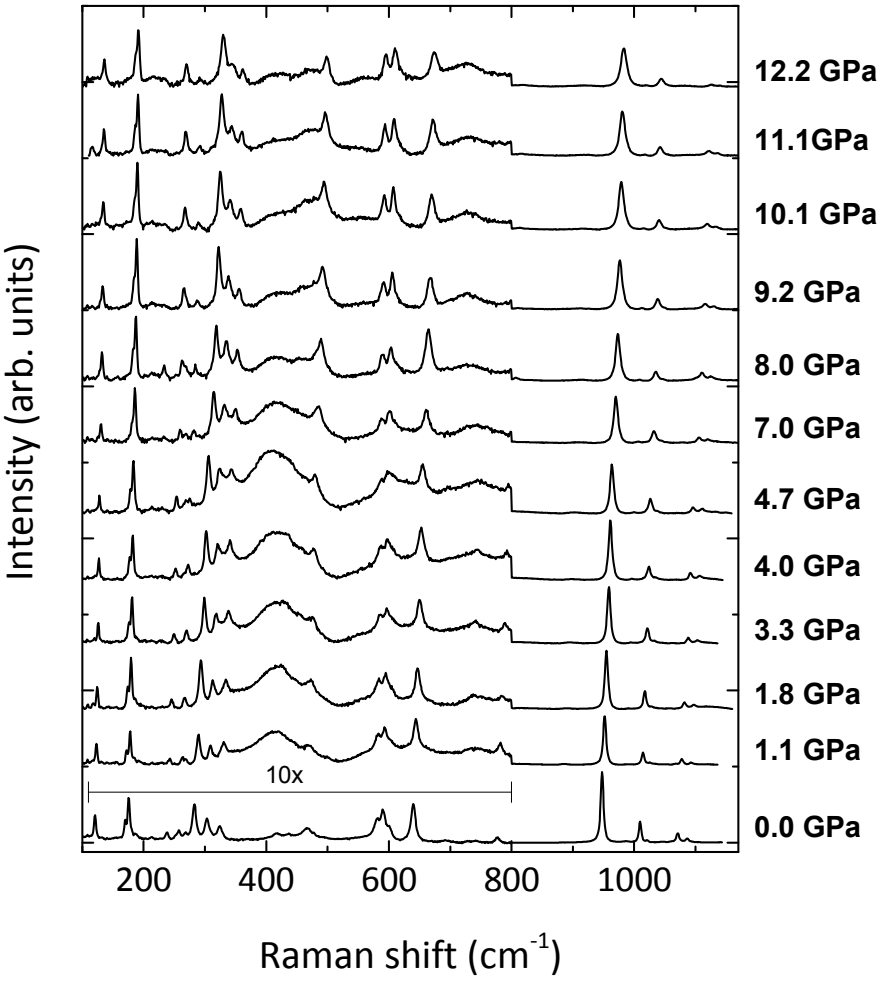

Figure S3. Raman spectra for α-$LiNiPO_4$ at selected pressures. Below 800 cm^{-1} all the spectra have been magnified 10x.

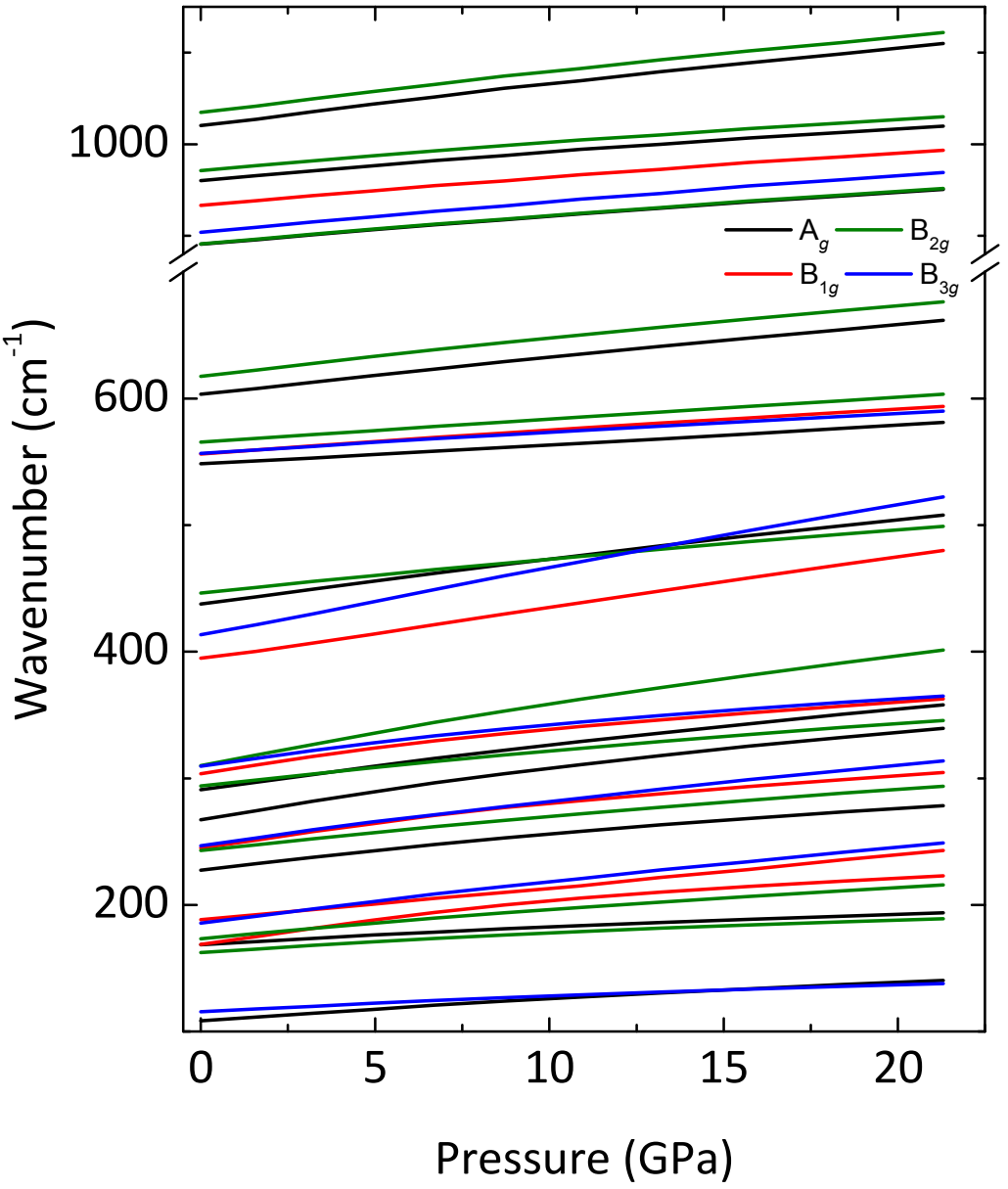

Figure S4. Theoretical pressure dependence of the calculated Raman modes of olivine-type $LiNiPO_4$.

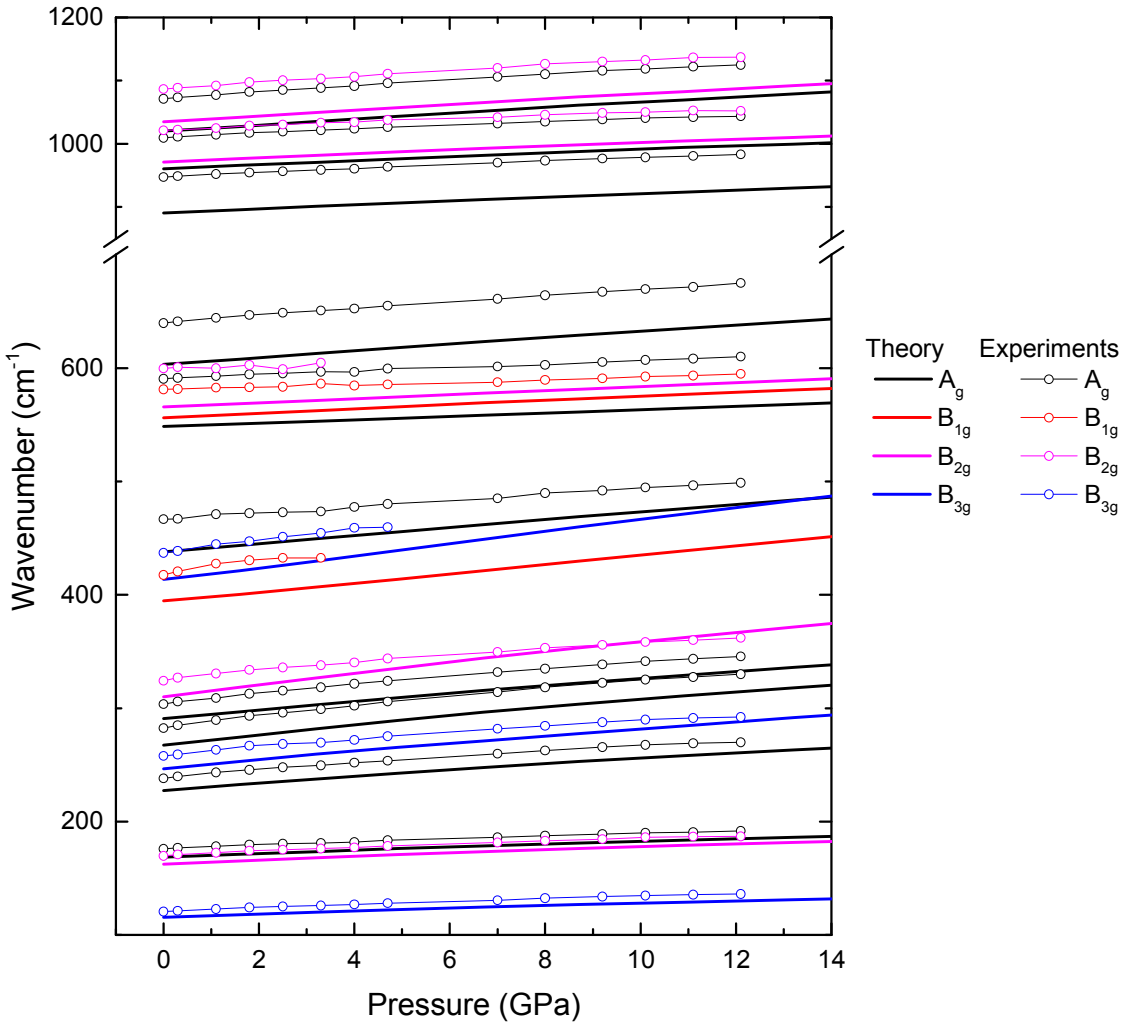

Figure S5. Comparison of the theoretical pressure dependence of the calculated Raman modes of olivine-type $LiNiPO_4$ (lines) and of the experimentally detected Raman active modes (open circles+lines). Only theoretical modes corresponding to actually detected modes (for P>10-4 GPa) are shown.

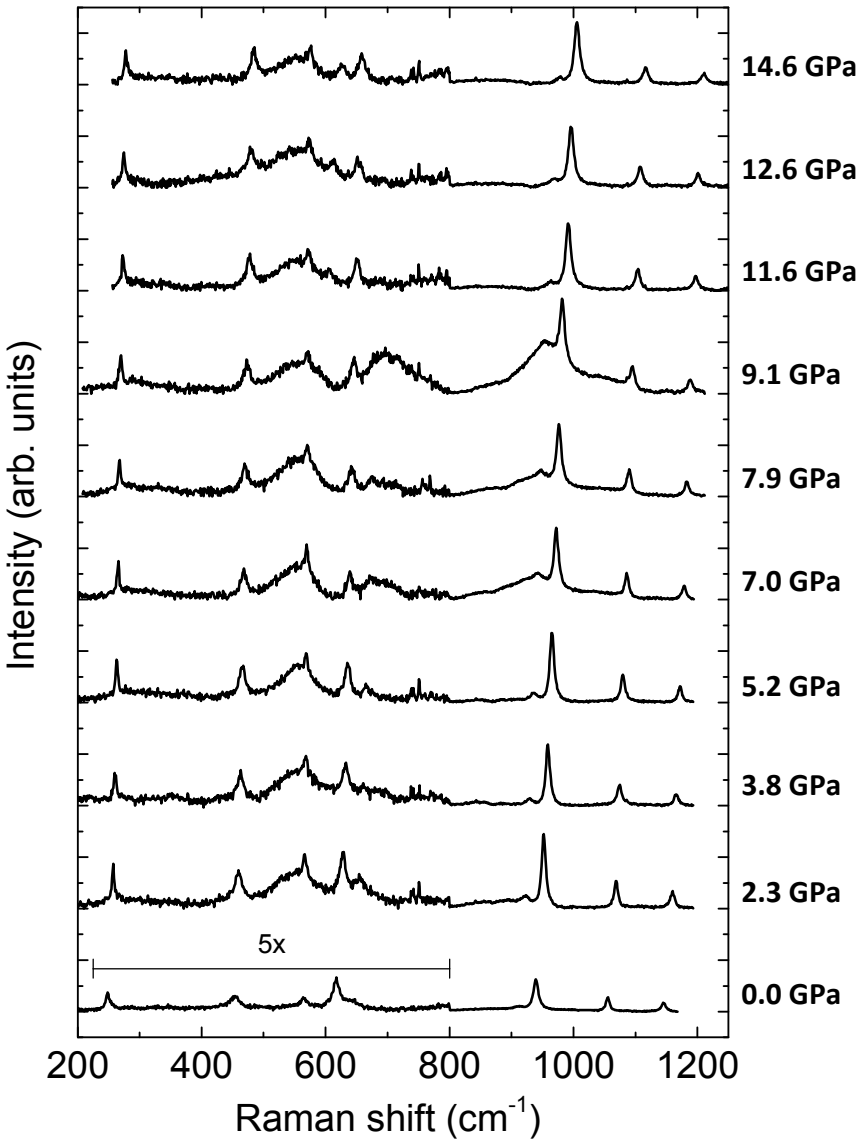

Figure S6. Raman spectra for β-$LiNiPO_4$ at selected pressures. To increase readability, all the spectra have been magnified 5x below 800 cm^{-1}.

Symmetry	IR shift (cm^{-1})	a_{teo} (cm^{-1} GPa^{-1})
B_{3u}	172.8	-0.8
B_{1u}	187.1	1.0
B_{1u}	199.1	3.9
B_{2u}	236.2	3.1
B_{3u}	241.0	3.1
B_{3u}	249.9	6.1
B_{2u}	309.5	2.7
B_{1u}	343.2	4.4
B_{2u}	382.4	6.3
B_{2u}	487.4	3.7
B_{1u}	497.2	12.4
B_{3u}	502.6	0.8
B_{2u}	573.0	2.2
B_{1u}	576.9	1.9
B_{3u}	863.6	4.7
B_{2u}	867.7	4.9
B_{2u}	1016.7	4.3
B_{1u}	1043.8	4.6

Table S2. Calculated IR phonons for the β-phase of $LiNiPO_4$.

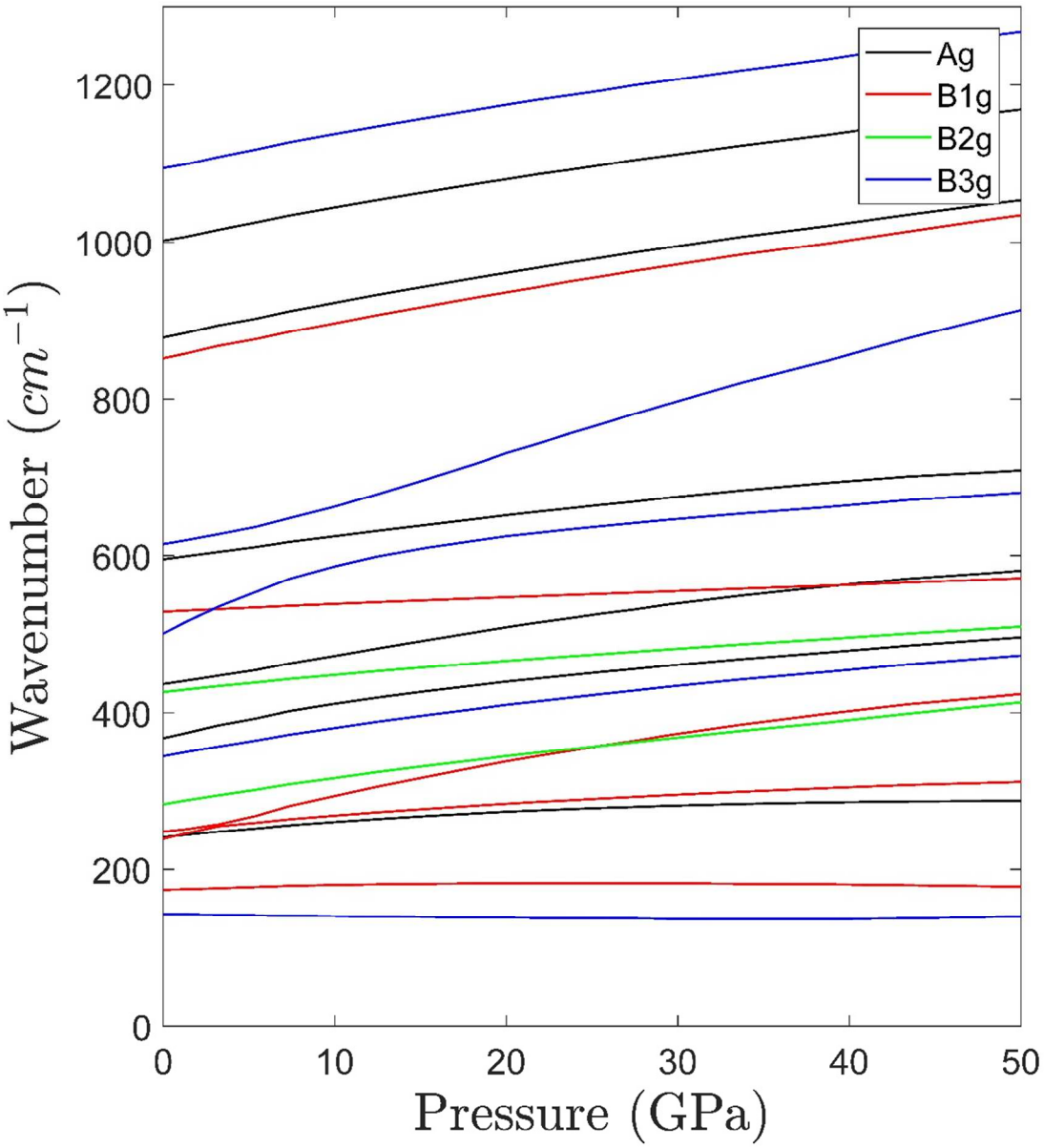

Figure S7. Theoretical pressure dependence of the calculated Raman modes of the β-phase of $LiNiPO_4$.

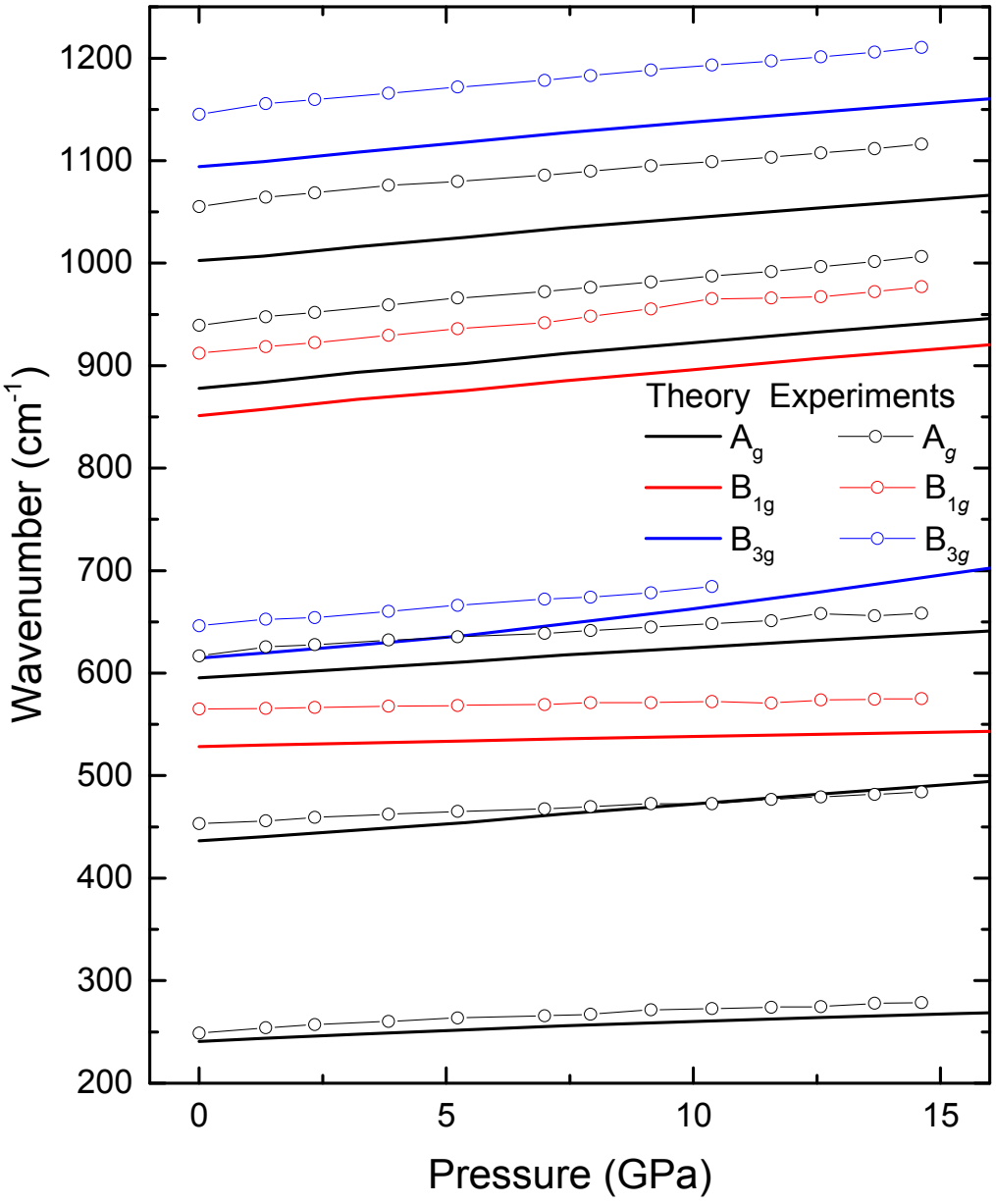

Figure S8. Comparison of the theoretical pressure dependence of the calculated Raman modes of β-LiNiPO4 (lines) and of the experimentally detected Raman active modes (open circles+lines). Only theoretical modes corresponding to actually detected modes (for $P>10^{-4}$ GPa) are shown.